University of South-Eastern Norway

www.usn.no

FMH606 Master's Thesis 2019
Electrical Power Engineering

Online monitoring and visualizing of a generator's capability with Simulink

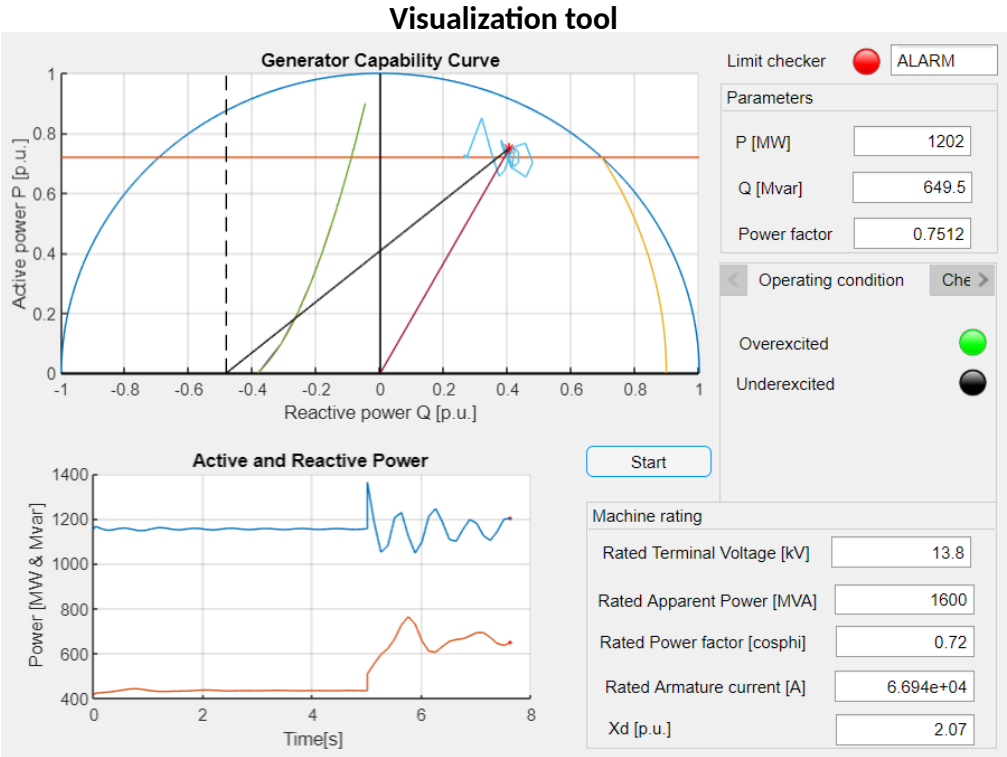

Prabesh Khadka

Faculty of Technology, Natural Sciences and Maritime Sciences

Campus Porsgrunn

University of South-Eastern Norway

www.usn.no

Course: FMH606 Master's Thesis 2019
Title: *Online monitoring and visualizing of a generator's capability with Simulink*
Pages: *93*
Keywords: *Voltage stability, Voltage collapse, Long-term dynamics, Generators capability curve*

Student: *Prabesh Khadka*
Supervisor: *Thomas Øyvang, Dietmar Winkler*
External partner: *Statkraft*
Availability: *Open*

Summary:
The power systems today are becoming more larger, complex and are operating closer to their security and stability limits particularly due to an increase in load demands and number of environmental concerns. Voltage stability has been a major subject of discussion and concern in electric power system operation and planning worldwide. Firstly, this thesis aims to do the survey on voltage stability and collapse phenomena in order to get insights into the mechanisms, causes, and prevention techniques to avoid such.

The dynamic long-term voltage stability analysis is carried out using a free and open source, MATLAB based-PSAT software taking a test power system. The influence of load models, overexcitation limiter and transformer load tap changers on voltage collapse are investigated as a part of the thesis. It is observed that the constant power load has a greater impact on the voltage instability as it tries to restore the load unlike constant impedance and the constant current loads.

Furthermore, a mathematical model for drawing the generator PQ capability diagram is presented and implemented in MATLAB software environment. For improved visualization and user interactions, a visualization tool is developed using the Graphical User Interface. In addition, the temperature development in the rotor and stator of the 103 MVA hydrogenerator at 'Åbjøra' in Norway, is investigated in the same visualization tool utilizing the already developed thermal model.

For increased accuracy of the results from dynamic voltage analysis, development and use of more accurate power system component models is recommended. Moreover, the effect of changing armature voltage and the direct axis synchronous reactance on PQ capability diagram can be investigated under further study.

Preface

This thesis is submitted to the University of South-Eastern Norway (USN) as the partial requirement for the fulfillment of the master's degree program in Electrical Power Engineering. The thesis was undertaken as a part of the course FMH606 starting January 2019 with Statkraft as the external partner. The eagerness to study about the role of reactive power in maintaining voltage stability in an AC electrical network and the generator's role in handling such is what motivated me to take this topic as my thesis work.

I would like to thank my supervisor Thomas Øyvang and co-supervisor Dietmar Winkler for their excellent guidance and valuable support throughout the work. Special thanks to Mr. Om Prakash Chapagain for giving valuable insights into mathematical computations and programming. Thanks to my friend Madhusudhan Pandey for his co-operation and support throughout this journey. Finally, sincere gratitude to my family for their continuous encouragement and support throughout the work.

Porsgrunn, 13th May 2019

Prabesh Khadka

Contents

List of Figures

List of Tables

List of Abbreviations

AVR	Automatic Voltage Regulator
CPF	Continuation Power Flow
EHV	Extra-high-voltage
FACTS	flexible Alternating Current Transmission System
GUI	Graphical User Interface
LTC	Load Tap Changing
OC	Open-circuit
OPF	Optimal Power Flow
OXL	Overexcitation Limiter
PMU	Phasor Measurement Unit
PSAT	Power System Analysis Toolbox
PSS	Power System Stabilizer
TCSC	Thyristor Controlled Series Capacitors
ZIP	Constant impedance, Constant current and Constant power load

List of Symbols

Symbol	Explanation	Unit
I	Armature current	$[A]$
I_{fd}	Rated field current	$[A]$
I_t	Rated armature current	$[A]$
P	Active power	$[W]$
Q	Reactive power	$[var]$
R_s	Stator winding resistance per phase	$[\Omega]$
T_r	Temperature of rotor	$[^\circ C]$
T_s	Temperature of stator	$[^\circ C]$
V	Terminal voltage (or U)	$[V]$
V	Terminal voltage	$[V]$
x_d	Synchronous reactance d-axis (or X_d)	$[p.u.]$
x_q	Synchronous reactance q-axis	$[p.u.]$
Z	Impedance	$[\Omega]$
θ	Load angle (or δ)	$[degrees]$
ϕ	Power factor angle	$[degrees]$

The phasors are indicated by a tilde symbol, e.g. $\tilde{I}$

1 Introduction

1.1 Background and objective

Voltage instability is becoming one of the major issues in power system operation and planning worldwide due to the increased power demand. Several voltage collapse incidents have been reported at different corners of the world and few examples can be found in CIGRE report [1]. The inability of the power system to meet the reactive power demand in an electrical network is one of the cause of voltage instability. Generators are normally the sources of reactive power support during voltage insecurities. So monitoring the voltage profiles, voltage regulation and the reactive power output of generators is one of the important countermeasures for voltage collapse.

In a recent Ph.D. study [2], utilization of the thermal capacity of a hydrogenerator to enhance the voltage stability of the power system was studied. The available voltage control capability depends upon the temperature rise of the machine during contingencies [2]. Furthermore, the normal limits of operation of generators without exceeding their thermal limitations is defined by the reactive capability curve. This thesis work will primarily address the implementation of PQ capability diagram for online monitoring of generator's capability. In addition, long term voltage stability or the collapse phenomenon which includes the dynamics of slow acting components such as load tap changers, generator excitation limiters and thermostat controlled loads will be studied.

1.2 Scope of work

In this thesis work, a survey on the voltage stability including power voltage characteristics of the network and the mechanisms of the voltage collapse phenomenon has to be carried out including its time domain characteristics. The large disturbance voltage stability shall be analyzed taking a standard 10-bus test system using time-domain simulations. Furthermore, an automatic visualization tool needs to be developed to monitor the capability of the generator present in the same test system.

The dynamic simulation of the test system will be carried out in MATLAB based power system toolbox PSAT, a Free and Open Source Software (FOSS) which includes different static and dynamic power system component models. Moreover, the PQ capability diagram will be implemented in the MATLAB programming language.

1.3 Outline of the thesis

The overall thesis work is presented in mainly seven chapters. Chapter 1 includes the introduction to the project. In Chapter 2, the background theories regarding the voltage stability and collapse phenomenon are reviewed followed by the description of some of the power system component models in Chapter 3.

Chapter 4 describes the simulation setup and description of the 10-bus test system, the used PSAT models, MATLAB setup for capability diagram and the Simulink setup for the thermal model of hydrogenerator described in Ph.D. thesis [3].

In Chapter 5, the results and discussions regarding the simulation are presented.

Chapter 6 gives the concluding remarks on the overall thesis work while in Chapter 7, the possible future works are recommended.

2 Theory

In this section, the basic theory and concepts related to voltage stability, collapse phenomenon and the synchronous generator PQ capability diagram has been described.

2.1 Voltage stability

The ability of a power system to maintain the steady acceptable voltage at all the buses during normal operating conditions and after being subjected to the disturbance can be termed as voltage stability [4]. Disturbances such as system faults, loss of generation or lines, an increase in load demand or change in system condition cause an uncontrollable drop in voltage and system enters into a state of voltage instability. The inability of the power system to meet the reactive power demand is the main reason for instability [4].

Figure 2.1 shows the classification of power system stability according to IEEE/CIGRE joint Task Force report [5]. This thesis work focuses on Long term voltage stability.

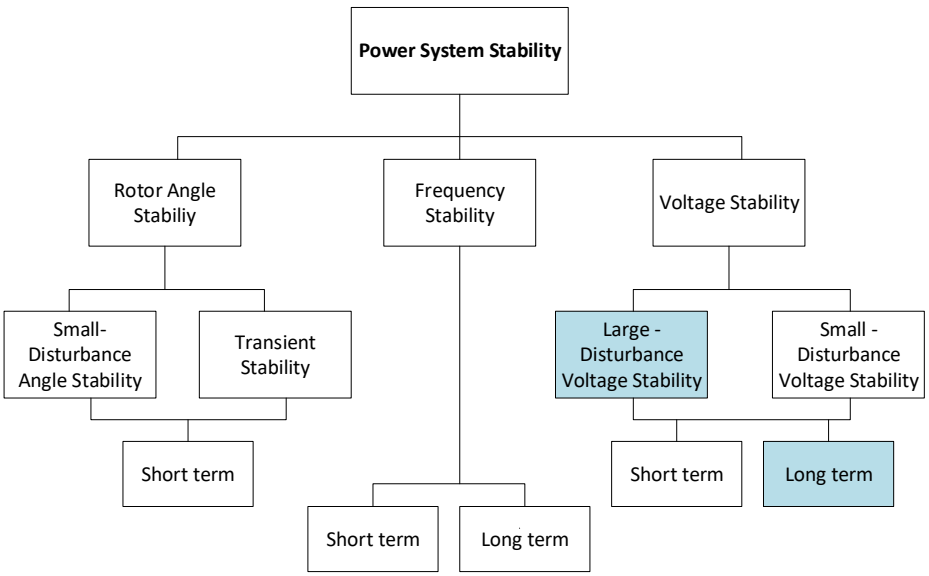

Figure 2.1: Classification of power system stability [5].

According to CIGRE definition [1], "*Voltage instability is the absence of voltage stability, and causes a progressive decrease (or increase).*"

The voltage stability limit or the margin of the system can be defined by determining the maximum amount of power that a system can supply to a load. The maximum power transfer level can be described by considering the following two terminal network of Figure 2.2.

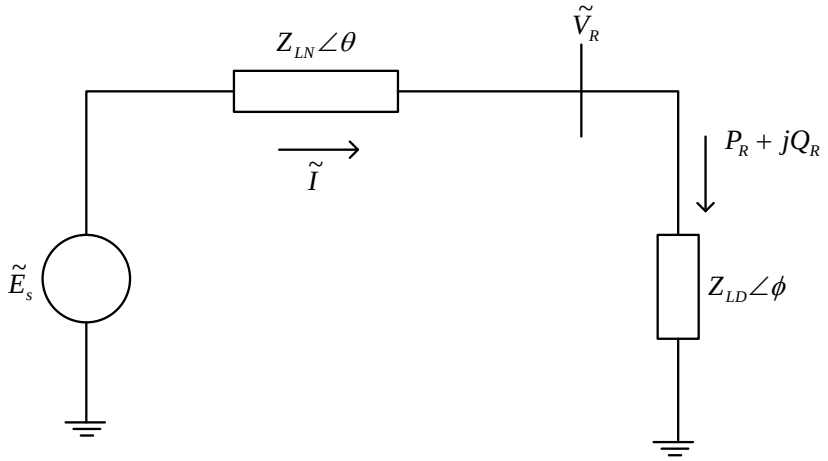

Figure 2.2: Equivalent circuit of a simple two bus system [4].

The expression for the current $\tilde{I}$ for Figure 2.2 is given by

$$\tilde{I} = \frac{\tilde{E}_s}{\tilde{Z}_{LN} + \tilde{Z}_{LD}} \tag{2.1}$$

where $\tilde{I}$ and $\tilde{E}_s$ are phasors, and

$$\tilde{Z}_{LN} = Z_{LN}\angle\theta,\ \tilde{Z}_{LD} = Z_{LD}\angle\phi$$

The magnitude of current is given by

$$I = \frac{E_s}{\sqrt{(Z_{LN}\cos\theta + Z_{LD}\cos\phi)^2 + (Z_{LN}\sin\theta + Z_{LD}\sin\phi)^2}}$$

This can be expressed in the following form

$$I = \frac{1}{\sqrt{F}}\,\frac{E_s}{Z_{LN}} \tag{2.2}$$

where

$$F = 1 + \left(\frac{Z_{LD}}{Z_{LN}}\right)^2 + 2\left(\frac{Z_{LD}}{Z_{LN}}\right)\cos(\theta - \phi)$$

The magnitude of the receiving end voltage is given by

$$V_R = Z_{LD} I = \frac{1}{\sqrt{F}} \frac{Z_{LD}}{Z_{LN}} E_s \tag{2.3}$$

The power supplied to the load is

$$P_R = V_R I \cos\phi = \frac{Z_{LD}}{F} \left(\frac{E_s}{Z_{LN}}\right)^2 \cos\phi \tag{2.4}$$

From basic circuit theory, it is evident that the power transfer to the load is maximum when the value of source impedance equals to the value of load impedance, that is when $Z_{LN} = Z_{LD}$. From equations 2.2 and 2.3, it can also be seen that the power-voltage characteristics of the system (P_R and V_R) depends upon the load power factor $\cos\phi$. Figure 2.3 shows the power-voltage characteristics for different values of load power factor [4]. The tip of this characteristic curve represents the maximum power transfer limit for a given load power factor.

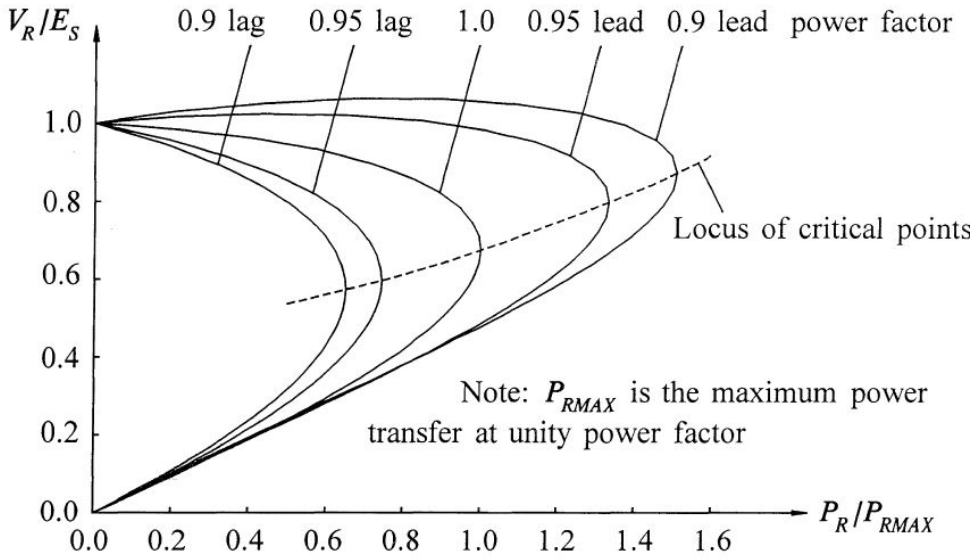

Figure 2.3: Power voltage characteristics of the system [4].

2.1.1 Study of voltage collapse phenomenon in time domain

The dynamics of voltage collapse could range from a few seconds to tens of minutes. So, depending upon the duration of dynamics, there are mainly two-time frames for voltage

stability namely transient and the long term [1]. Figure 2.4 shows a time response chart which includes different system components and their time responses that characterize the difference between transient and the long-term phenomena.

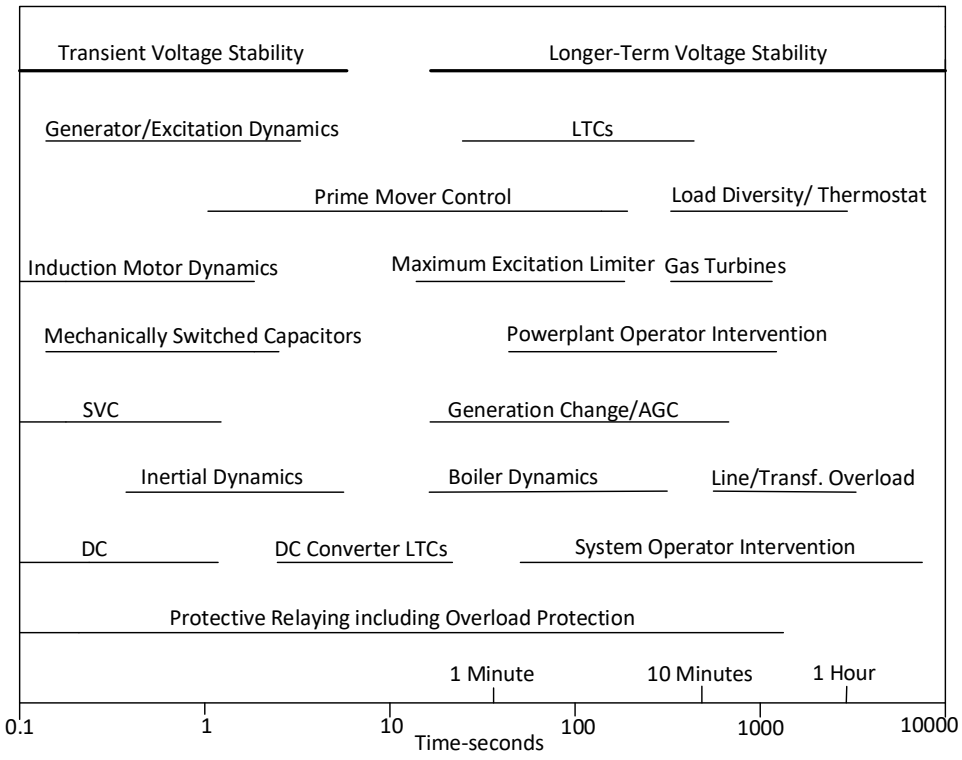

Figure 2.4: Voltage stability phenomena and time frames [6].

The two important definitions are as follows:

- Transient voltage collapse includes the dynamics of fast acting loads such as induction motor or HVDC converters and the time period is one to several seconds.

- Long term voltage collapse involves slow acting load components such as LTC[1] transformers, thermostat-controlled loads and generator excitation limiters. The time frame ranges from 0.5 to 30 minutes [1].

.

[1]The Load tap changing (LTC) is also sometimes referred by other names such as On-load tap changing (OLTC) and Under-load tap changing (ULTC).

2.1.2 Mechanism of voltage collapse

Different network components are responsible for the long-term voltage collapse phenomenon. Following are some components which play an important role in the reactive power balance process in the network.

Generators

During normal operating conditions, the generator's AVRs maintains the terminal voltage constant. Following the disturbances in the network, the system voltages falls and during such conditions, the reactive power demand on generators might exceed field current limits. The overexcitation limiters (OXL) limits the generator's field current automatically according to its characteristics [4]. The generator terminal voltage decreases when it reaches its reactive power output limit. Now the other generators in the network try to meet the increased reactive power demand and this might lead to cascading overloading of generators. Only a few generators remain which can help in controlling the voltage and are situated far away from the load center. The effectiveness of the shunt capacitors is also reduced at reduced transmission voltage. In such situation, the system is likely to undergo voltage instability and is prone to voltage collapse [7].

Transformer On-load tap changers

The automatic load tap changers normally keep the distribution voltage at a constant value by adjusting its taps. The loads are restored to a pre-fault level following a disturbance and after some time delay [1]. This resulting increment in load causes increases in MWs, Mvar's, losses in the EHV lines which would ultimately cause high voltage drops in the line. Therefore, the reactive power output from all the generators would increase with each tap-changing operation and when the generators reache their reactive power capability limits, the system is on the verge of voltage instability [8].

Loads

Normally the voltage dependency of loads helps to stabilize the system after an event of disturbance or a fault in a system [1]. With the drop-in voltage, residential active and reactive loads decreases and this will helps to reduce line loading and reactive power losses. But the industrial loads with a large share of induction motors causes a net increase in the reactive load as the reactive output of capacitors decreases with a decrease in voltage [4].

Thyristor controlled loads try to restore the load at the event of low voltage and act as a constant power load. That means loads try to restore the consumed power to the prefault level when voltage drops at the buses. This results in the increased load current and in turn, decreases the load bus voltage further [9].

Asynchronous motors, on the other hand, draw high reactive current when the voltage goes down to 85 to 90 % of the rated value [4]. The simultaneous acceleration of all the motors after the fault clearance would increase the reactive loads significantly in the network. This, in turn, causes a further drop in bus voltages [1].

So proper load modelling is very important factor to be considered while studying voltage stability and collapse phenomenon which is further described in Section 3.1.

2.1.3 Approaches to voltage stability analysis

There are various methods for analyzing voltage stability. All these methods can be broadly classified into two major categories as static analysis and the dynamic analysis [10]. In this thesis work, a dynamic time-domain simulation was performed taking a simple test system which will be further described in Section 4.2.1.

Static analysis

The static approach uses the system conditions or snapshots at various time frames to evaluate the voltage stability [4]. Some of the approaches which are described in [11] are listed below.

- P-V Curve method
- Q-V Curve method
- Modal Analysis
- Sensitivity Analysis

These approaches or methods uses less computational time and are easier to implement [11]. However, when determining the PV curve there will be a problem in the convergence of power flow solution close to the point of voltage collapse as Jacobian matrix of the system becomes singular at that instant [9].

Dynamic analysis

In contrast to the static analysis, dynamic approaches give the detail events and their chronology which leads to the voltage instability and the collapse [4]. However, the time domain simulations are time-consuming as larger time constants are involved and the detail dynamics of various power system component models such as ULTC, excitation system limiters, dynamic loads, are considered during simulation [9].

A new approach of using combined static and dynamic approach for voltage stability analysis has been presented in paper [11].

2.2 Generator power capability

Synchronous generator is a primary source of reactive power in the network and plays an important role in maintaining the voltage stability in the network. The boundaries for supplying the reactive power at a given active power output is defined by the generator capability curve provided by the manufacturers [12]. The generator capability diagram provides a boundary within which the generator can operate safely without exceeding the thermal limitations. Moreover, another important role of the capability curves is the proper settings of the relays used in the protection of synchronous generator such as AVR, under-excited controllers, overexcitation limiter, loss of field relay [13].

Synchronous generator is a source of active as well as reactive power which can be controlled over a wide range of values. The active power P and reactive output power Q for round-rotor generators ($x_d = x_q$) when neglecting the resistance (r=0) for the generator-transformer unit as shown in Figure 2.5 can be expressed as the following equations [14].

$$P = \frac{E_q V}{x_d} \sin\delta \tag{2.5}$$

$$Q = \frac{E_q V}{x_d} \cos\delta - \frac{V^2}{x_d} \tag{2.6}$$

where,
$x_d = X_d + X_T$ = direct axis synchronous reactance.
x_q = quadrature axis synchronous reactance.
$r = R + R_T$ = generator resistance when added to the transformer resistance.
E_q = air-gap electromotive force (emf).
V = voltage on the terminal of step-up transformer.
δ = power angle of generator.

Figure 2.6 shows the synchronous generator capability diagram where the area bounded by the curve $ABCDEFG$ indicates the safe region of operation for salient-pole machine.

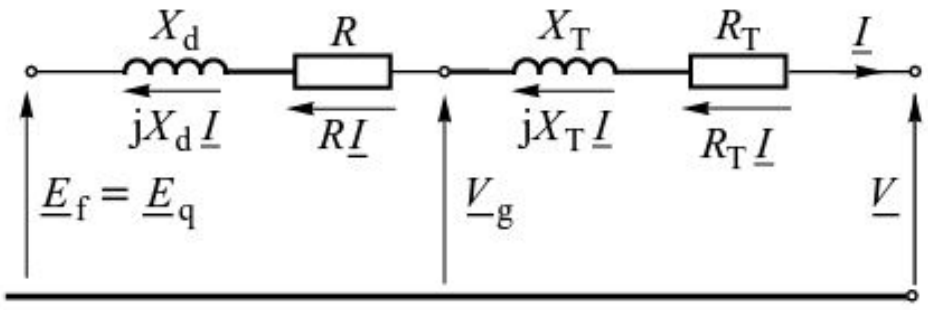

Figure 2.5: Equivalent steady state circuit diagram for round rotor generators with a step-up transformer [14].

Following operational constraints are the reasons for the limits in active and reactive power of the synchronous generator [14].

1. Armature current limit.
2. Field current limit.
3. Steady-state stability limit.
4. Stator end region heating limit.
5. Generator active power limit.

Armature current limit

The armature current I causes I^2R power loss in the armature winding which then increases the temperature in the windings. So, this current should be smaller than a certain maximum value I_{max} in order to limit the temperature rise.

The active and reactive power is given by $P = VI\cos\phi$ and $Q = VIsin\phi$ respectively. Squaring and adding these two equations yields, $P^2 + Q^2 = (VI)^2$ which represents the equation of a circle in the $P-Q$ plane with centre at origin and radius VI [14].

For a given voltage V and loading $I = I_{max}$,

$$P^2 + Q^2 = (VI_{max})^2 \tag{2.7}$$

which is as shown by curve-1 in Figure 2.6.

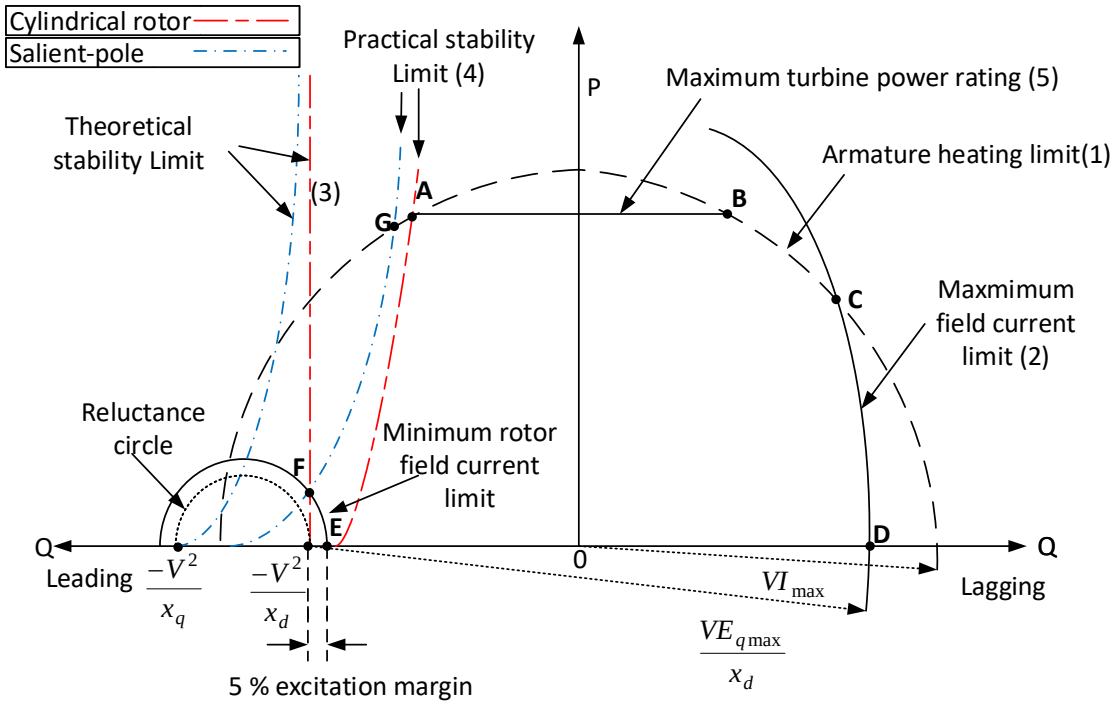

Figure 2.6: Capability diagram of synchronous generator [9], [15].

Field current limit

The field winding gets heated because of I_f^2 power loss. So, to keep the temperature within the certain limit in field windings, the field current I_f should be less than certain maximum value say I_{fmax}. By manipulating the equations 2.5 and 2.6, following relations can be obtained [14],

$$P = \frac{E_q V}{x_d} \sin\delta \tag{2.8}$$

$$Q + \frac{V^2}{x_d} = \frac{E_q V}{x_d} \cos\delta \tag{2.9}$$

Squaring and adding above two equations yields:

$$P^2 + \left(Q + \frac{V^2}{x_d}\right)^2 = \left(\frac{E_q V}{x_d}\right)^2 \tag{2.10}$$

For $E_q = E_{qmax}$,

$$P^2 + \left(Q + \frac{V^2}{x_d}\right)^2 = \left(\frac{E_{qmax}V}{x_d}\right)^2 \tag{2.11}$$

Equation 2.11 represents a circle with center $(0,-\frac{V^2}{x_d})$ and radius $\frac{E_{qmax}V}{x_d}$ in $P-Q$ plane as shown by curve-2 in Figure 2.6.

Steady-state stability limit

For the stable operation of generators, the power angle δ should be within the limit and the theoretical stability limit occurs when $\delta = 90°$. Dividing equation 2.8 by 2.9 following equation can be obtained:

$$P = \left(Q + \frac{V^2}{x_d}\right) \tan\delta \tag{2.12}$$

Putting $\delta = \delta_{max}$ gives,

$P = mQ + c$ where slope $m = \tan\delta$ and intercept c= $\frac{V^2}{x_d}\tan\delta$.
So, theoretical stability limit can be represented by a straight line which intersects the reactive power axis at a point $P = 0$ or $Q = -\frac{c}{m} = -\frac{V^2}{x_d}$ as shown in Figure 2.6 (line-3).

But in practice, in order to allow the load increase of either 10 or 20 % before instability, a safety margin is always introduced [16]. So, practical stability limit can be obtained by reducing the active power output by 10% of the rated power at constant field current [9] as shown by curve-4 in Figure 2.6.

Stator end region heating limit

This constraint is due to the localized heating at the end region of the armature during under-excited operation of the synchronous generator. During under-excitation operation, the field current is low so the retaining ring is not saturated as well as the flux produced by the armature current gets added up to the flux produced by the field current during this condition. Hence, armature end-turn leakage flux gets enhanced and results in the heating effects at the end regions due to the eddy current produced in the stator core laminations because of these fluxes entering and leaving in a perpendicular direction especially in the round rotor machine [4].

The end-region heating limit is determined experimentally by the manufacturer [14].

Generator active power limit

The generator active power limit is limited by the turbine power and depends upon the type of turbine. The two turbine limits; upper P_{max} and the lower limit P_{min} can be represented by two lines parallel to Q-axis in the $P-Q$ plane. Line-6 in the Figure 2.6 represents the upper constrain due to maximum turbine power rating [14].

The area bounded by the bold lines in Figure 2.6 represents the safe region of operation. It can also be noted that the first three limitations described above depend upon the terminal voltage V. That means the change in terminal voltage affects the center and radius of the circle as well as the position of the straight lines and ultimately the area of safe operation [14].

3 Modelling of power system components

In this chapter, two of the important power system component models; load models and the under-load tap changer has been discussed. These components have a significant role in long-term voltage stability analysis of a power system. In addition, an already developed online low order thermal model of a hydrogenerator based on [2] has also been described.

3.1 Load models

There are generally two types of load models: static and dynamic load models which are further described in this section [4]. Out of two types, only the effect of static load models on voltage stability has been taken as a part of the study in this research work.

Static load modelling

In this modelling technique, loads are modelled as algebraic functions of the bus voltage magnitude and frequency at some instant of time [4]. Exponential load model, polynomial or ZIP model, frequency-dependent load model, piecewise approximation are some types of mathematical models which reflects various load behaviours [14].

The polynomial or the ZIP model is represented by the following equation [4]:

$$\begin{aligned} P &= P_0[p_1\bar{V}^2 + p_2\bar{V} + p_3] \\ Q &= Q_0[q_1\bar{V}^2 + q_2\bar{V} + q_3] \end{aligned} \tag{3.1}$$

where,
$\bar{V} = \frac{V}{V_0}$; subscript 0 represents variables at initial operating condition.
P and Q represents the active and reactive power consumption by the load at particular bus when bus voltage is V.
p_1, p_2, p_3 and q_1, q_2, q_3 are the proportion of active and the reactive power representing constant impedance, constant current and constant power respectively.

The frequency dependent load is characterized by multiplying the exponential model or ZIP model by some factor as shown below [4]:

$$\begin{aligned} P &= P_0[p_1\bar{V}^2 + p_2\bar{V} + p_3][1 + K_{pf}\Delta f] \\ Q &= Q_0[q_1\bar{V}^2 + q_2\bar{V} + q_3][1 + K_{qf}\Delta f] \end{aligned} \tag{3.2}$$

where,
Δf is the frequency deviation $(f - f_0)$.
K_{pf} and K_{qf} ranges from 0 to 3.0 and -2.0 to 0 respectively [4].

Following equation depicts the exponential load model:

$$\begin{aligned} P &= P_0 \left(\frac{V}{V_0}\right)^a \\ Q &= Q_0 \left(\frac{V}{V_0}\right)^b \end{aligned} \tag{3.3}$$

where, a and b are the parameters of the model which represents constant impedance, constant current and constant power characteristics of load for the values 0,1 and 2 respectively [4].

Dynamic load models

The areas like studies of inter-area oscillations, voltage stability, and long-term stability demands the dynamics of load components to be studied. The dynamic characteristics of the motor load is an important aspect of voltage stability studies as it occupies a large percentage of total power consumption in the power system.

Other dynamics aspects includes the extinction of discharge lamps, operation of protective relays, thermostatically controlled load and the response of LTCs [4].

3.2 Under load tap changer

in Section 2.1.2, influence of LTC transformer on voltage collapse has been described. The factors governing a tap changing operation are step size, time constant, reference voltage, and deadband. The load side voltage is monitored by a voltage relay and if voltage goes outside of the deadband, a timer relay is energized. The tap changing mechanism starts when the relay's time delay exceeds (after tens of seconds) and process of tap changing goes on until minimum or maximum tap is reached or until the voltage goes within the

band limit. After the voltage comes within the bandwidth, the timer mechanism and voltage relay are reset [17].

Usually the LTC transformers possess tap range of ±10% consisting of thirty-two steps each of 5/8%. A certain time delay in the range of 10-120 seconds before the tapping is allowed out of which the typical time delay is 30 to 60 seconds [17].

The detail model of LTC used for the simulation test case shall be discussed in the Section 4.2.2.

3.3 Thermal model of a hydrogenerator

In this section, typical power losses in the synchronous generator and the online thermal model based on [3] is described. The operational losses associated with the synchronous generator are the main inputs to the thermal model. The scope of this thesis work covers the visualization of the generator temperature variations in the visualization tool.

3.3.1 Copper losses

Copper losses comprise resistive heating losses in the stator and rotor windings of the machine. The three-phase stator DC-copper losses P_s can be obtained by using the following equation [2].

$$P_s = 3 \cdot R_{s_{(DC)}} \cdot I_t^2 \tag{3.4}$$

where, $R_{s_{(DC)}}$ represents the resistance of the stator winding per phase. The total rotor copper losses P_r can be obtained by using the following relation [2]:

$$P_r = 1.1 \cdot R_r \cdot I_{fd}^2 \tag{3.5}$$

where, R_r and $R_{s_{(DC)}}$ are the corrected resistances of the rotor winding and stator winding according to the reference temperature for different class of insulation system [18].

3.3.2 Iron losses

Iron losses P_{Fe} comprises of hysteresis losses and eddy current losses. Hysteresis loss depends upon the frequency and the value of maximum flux density per pole whereas the eddy current loss depends upon the square of the frequency and maximum flux density [19].

3.3.3 Stray losses

Stray losses are caused by non-sinusoidal, non-fundamental flux density variations. It consists of the losses related to eddy current losses in the stator windings, stator end region losses and the losses related to damper bars in the rotor laminations [19].

3.3.4 Mechanical losses

The mechanical losses P_v includes the losses related to friction in bearings and windage. Windage losses are present in the cooling fans and the rotor blades [19].

Figure 3.1 shows the schematic diagram of the proposed online monitoring algorithm based on [3]. It clearly shows how the model inputs- field current of the machine I_{fd}, terminal current I_t, the speed of the machine ω and machine terminal voltage V_t, relates to the corresponding temperatures via the machine losses.

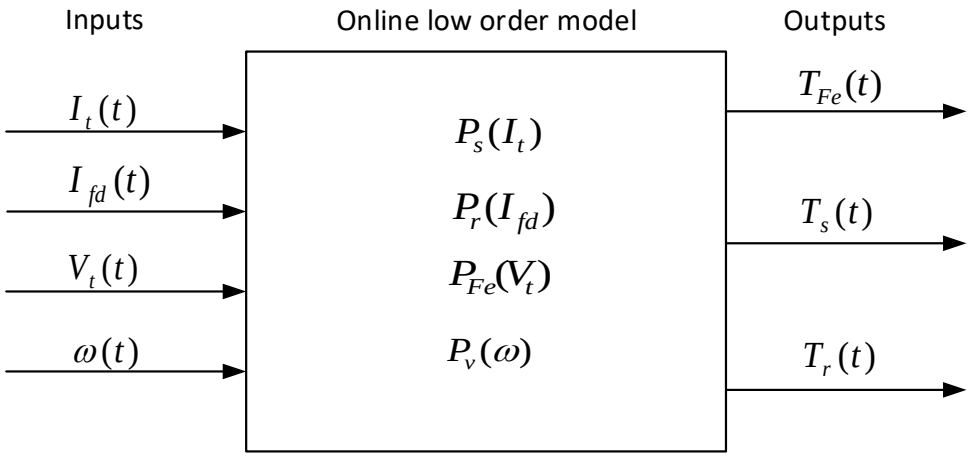

Figure 3.1: Schematic diagram of online low order thermal model [3].

The three governing differential equations defined in [3] for online monitoring of temperatures are as follows:

$$\frac{dT_r}{dt} = \frac{1}{\tau_{T,r}}[\Delta P_r R_r - (T_r - T_{1,o})] \tag{3.6}$$

$$\frac{dT_s}{dt} = \frac{1}{\tau_{T,s}}[\Delta P_s R_s - (T_s - T_{Fe})] \tag{3.7}$$

$$\frac{dT_{Fe}}{dt} = \frac{1}{\tau_{T,Fe}}[\Delta P_{Fe} R_{Fe} + \frac{R_{Fe}}{R_s}(T_s - T_{Fe}) - (T_{Fe} - T_\delta)] \tag{3.8}$$

where, T_r, T_s and T_{Fe} represents the temperature of rotor winding, stator winding and the stator iron respectively.

4 Simulation

In this chapter, simulation setup for the Kundur 10-bus test system which has been used for long-term voltage stability study, and the visualization of generator's capability curve has been discussed.

The simulation for the study of long-term voltage stability phenomenon has been carried out using the Power System Analysis Toolbox (PSAT). In addition, the mathematical approach of drawing generator capability diagram in MATLAB software environment has been presented. The section also describes the methodology applied for the development of automatic visualization tool in MATLAB using Graphical User Interface.

4.1 Power System Analysis Toolbox (PSAT)

PSAT is a MATLAB based toolbox for the analysis and control of electric power system. It includes power flow, continuation power flow, optimal power flow, small signal stability analysis, and time domain simulation. It provides Graphical user interfaces (GUIs) to access all its functions as shown in Figure 4.1 and a Simulink-based library that allows easy access of tools required for the network design. The single line diagram drawn using Simulink library is loaded first through data file field of GUI and required analysis as listed below is carried out as simulation. Power flow Analysis is the core of the PSAT which allows to initialize the algebraic variables and the states after which further static or dynamic analysis can be performed. Some of the features are as follows [20].

1. Continuation power flow.
2. Optimal power flow.
3. Small signal stability analysis.
4. Time domain simulations.
5. Phasor measurement unit (PMU) placement.

Furthermore, PSAT contains various static and dynamic component models for power system analysis, out of which some component models has been used for this particular case study of long term voltage stability phenomenon. The models are as follows:

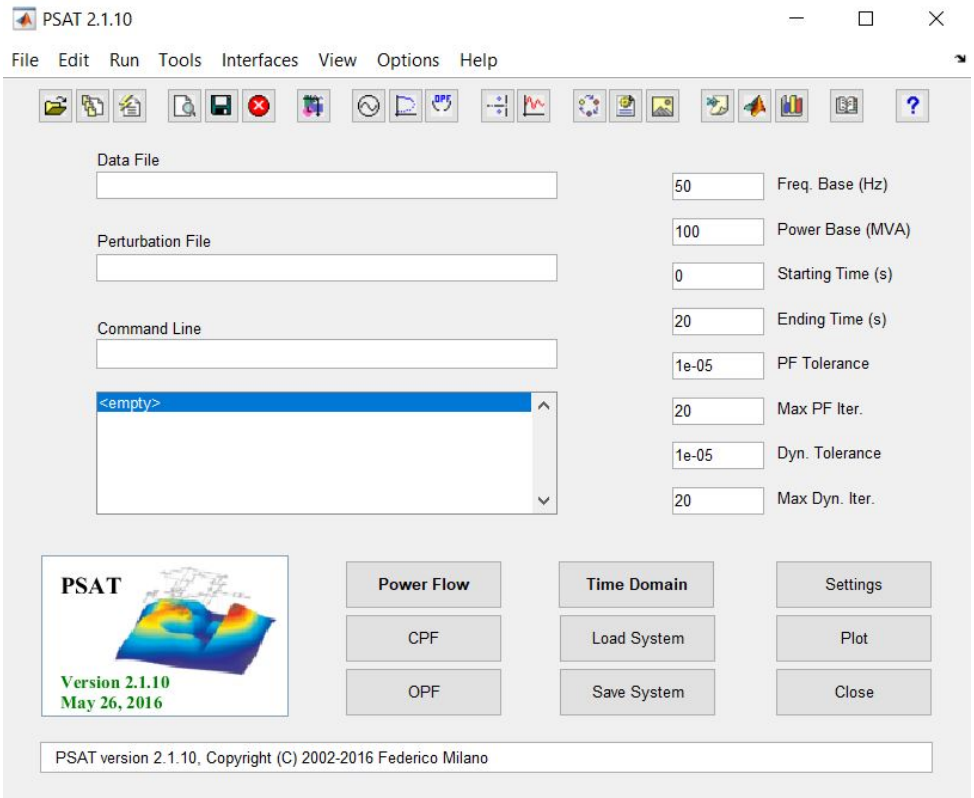

Figure 4.1: Graphical User Interface of PSAT [20].

1. *Power flow Data*: Bus bars, Transmission lines and transformers, slack buses.
2. *CPF and OPF Data*: Power supply bids and limits, generator power reserves.
3. *Switching operations*: Transmission line faults and breakers.
4. *Measurements*: PMU and bus frequency.
5. *Loads*: Voltage and the frequency dependent loads, ZIP loads.
6. *Machines*: Synchronous machines and induction motors.
7. *Controls*: Turbine Governors, AVR, PSS, OEL
8. *Regulating Transformers*: Load tap changers and phase shifting transformers.
9. *FACTS*: Static Var Compensators, Unified power flow controllers, TCSCs.
10. *Wind Turbines*: Constant and variable speed wind turbine models.
11. *Other models*: Solid Oxide Fuel Cell, sub-synchronous resonance model

4.2 Case Study: Kundur 10-bus test system

In this section the overall layout of the test system and the different power system component models used in same system has been presented. The models described are based on the PSAT models.

4.2.1 Description of a test system

This small test system has been studied in order to analyze the performance and influence of different power system components in voltage stability. The test system used for the study is actually based on the system described in [21] as BPA[1] test system, with some changes in load and compensating devices parameters. The single line diagram of the test system is shown in Figure 4.2. The necessary data used for the simulation of the system is provided in the Appendix B.

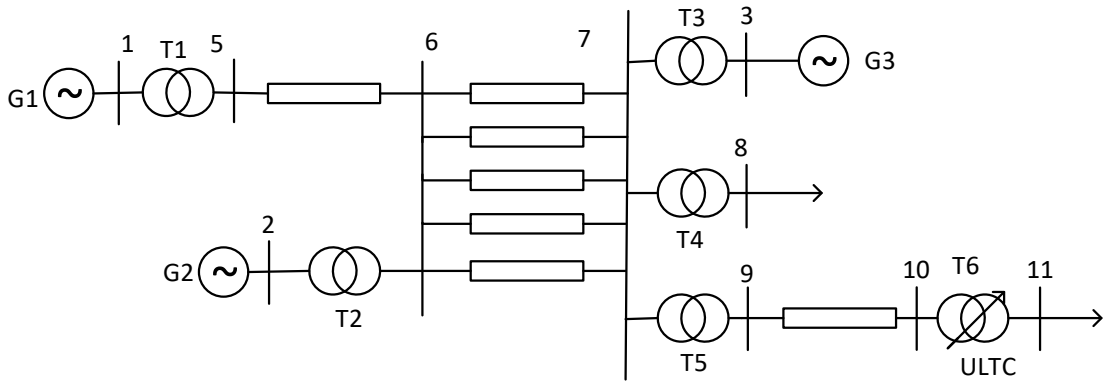

Figure 4.2: Single line diagram of test system [21].

Here the generators G1 and G2 in remote areas supply loads to the local area through five 500 kV transmission lines. The local generator G3 at bus 3 generates 1154 MW and the remaining power is supplied by two remote generators. Shunt capacitors are placed at various locations in the local area. Figure 4.3 shows the implementation of test system in PSAT. The load flow result is provided in Section 5.1.

[1]Bonneville Power Administration `https://www.bpa.gov`

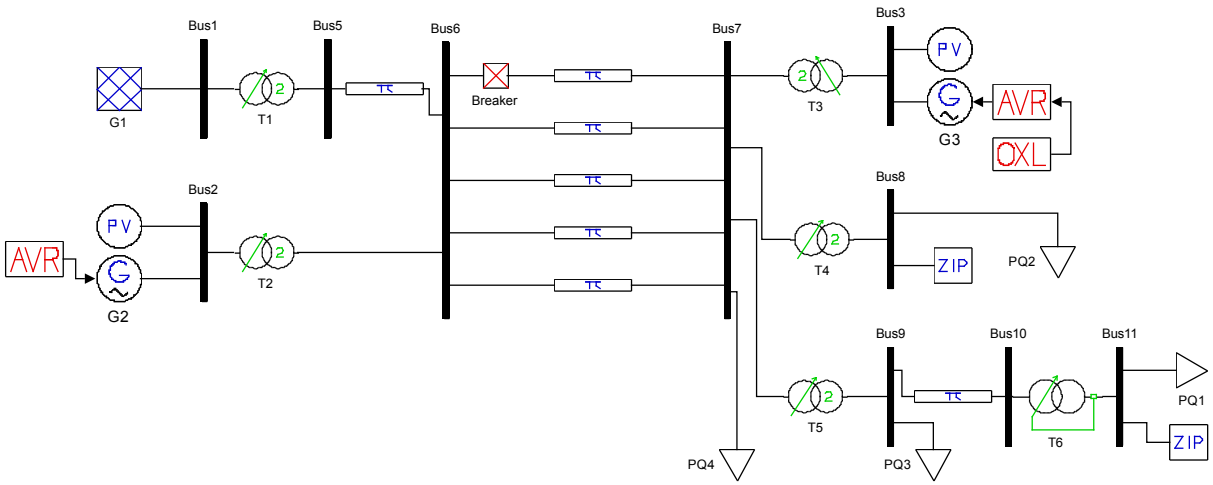

Figure 4.3: Single line diagram implementation of test system in PSAT.

4.2.2 System modelling

For the test system, the loss of one of the transmission lines between bus 6 and bus 7 is considered as a disturbance during the simulation.

Generators G2 and G3 are modelled using 6^{th} order model of PSAT whereas the generator G1 is modelled as an infinite bus.

Load at bus 8 is modelled as constant power for both active and reactive power whereas the load at bus 11 is modelled as constant impedance load for both active and reactive power as represented by PQ2 and PQ1 load respectively in Figure 4.3. The shunt capacitors at buses 7, 8 & 9 are modeled as PQ load (PQ4, PQ2, PQ3) respectively with the values presented in Table B.4.

Transformer LTC performance is characterized by deadband and step size. The deadband is taken as $\pm 1\%$ p.u. of bus voltage to which LTC is controlling and the tap range is ± 16 steps with a step size of $5/8\%$. The integral deviation H and inverse time constant K for the system is taken as 0.001 p.u. and 0.10 per second respectively.

Figure 4.4 and Figure 4.5 shows the equivalent π circuit model and secondary voltage control scheme of LTC transformer respectively. If the tap ratio step Δm is set as zero ($\Delta m = 0$), then

$$\tilde{m} = m, \tag{4.1}$$

Following equations exists for voltage and reactive power control:

$$\dot{m} = -Hm + K(v_m - v_{ref}) \tag{4.2}$$

$$\dot{m} = -Hm + K(q_{ref} + q_m) \tag{4.3}$$

where H is the integral deviation, K is the inverse time constant, v_m is the secondary voltage and v_{ref} is the reference voltage.

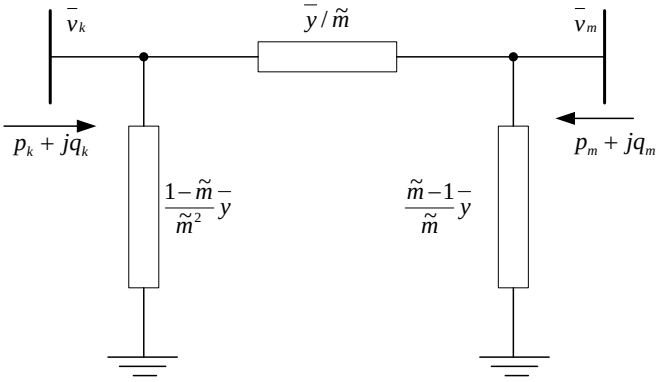

Figure 4.4: Equivalent π circuit of Under Load Tap Changer [20]

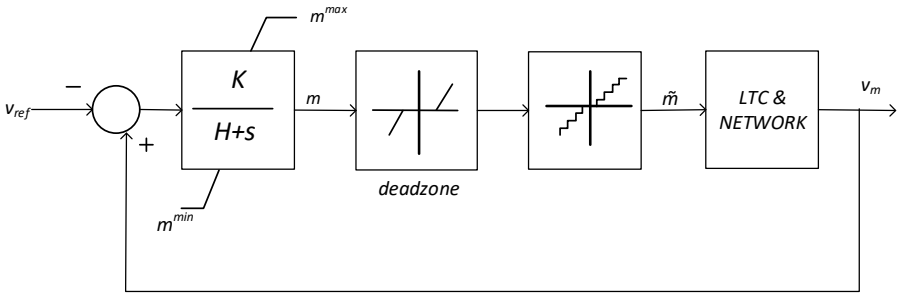

Figure 4.5: Secondary voltage control scheme of LTC [20].

Over Excitation Limiter is included for generator G3 only, for this case study. OXL acts when the field current is out of the acceptable limits. The response time of OXL depends upon the actual field current value. The higher the field current, the faster will be the response of OXL which then tries to reduce the field current within its limit. If the field current is less than or equal to its limit, OXL output signal will be zero; that means OXL does not operates.

OXL provides an additional signal v_{OXL} to the reference value of AVR. The AVR Type I of PSAT model is used for both the generators. The detailed model can be found in PSAT manual [20]. The OXL has been modeled as a pure integrator with anti-windup limits. When the field current is greater than its thermal limit ($i_f > i_f^{\mathrm{lim}}$) , OXL outputs some signal v_{OXL} to the summing block of AVR as shown in Figure 4.6 [20]. The integrator time constant T_o for the limiter is taken as 60 seconds whereas the maximum field current limit is chosen as 11.7 p.u. for the test system.

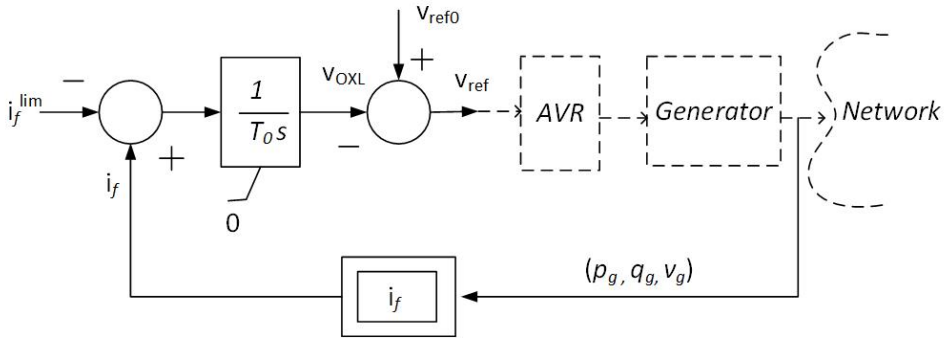

Figure 4.6: Over excitation limiter [20].

The equations that characterizes the operation of overexcitation limiter as shown in Figure 4.6 are as follows:

$$\begin{aligned} \dot{v}_{\mathrm{OXL}} &= (i_f - i_f^{\mathrm{lim}})/T_0 \quad \text{if } i_f > i_f^{\mathrm{lim}} \\ \dot{v}_{\mathrm{OXL}} &= 0 \qquad\qquad\qquad\quad \text{if } i_f \leq i_f^{\mathrm{lim}} \end{aligned} \tag{4.4}$$

Each overexcitation limiter model has following algebraic equations:

$$0 = \sqrt{(v+\gamma_q)^2 + p^2} + (\frac{x_d}{x_q} + 1)\frac{\gamma_q(v+\gamma_q) + \gamma_p}{\sqrt{(v_g+\gamma_q)^2} + p^2} - i_f \tag{4.5}$$

$$0 = v_{ref}^0 - v_{\mathrm{ref}} + v_{\mathrm{OXL}} \tag{4.6}$$

where,

$$\gamma_p = x_p/v$$
$$\gamma_q = x_q/v$$

v, p, and q are voltage, active and the reactive power of the generator respectively whereas x_d and x_q are direct axis and quadrature axis reactances of the generator to which OXL is connected respectively.

4.3 On-line PQ diagram

The theoretical PQ diagram is developed from the phasor diagrams of operation for both the salient pole rotor and the cylindrical rotor machines [22]. Active power, field current, stator current, frequency, terminal voltage, rated power of the turbine, heating-up of stator core end region and stability limits are the parameters which defines the operation of these machines.

The theoretical PQ diagram can be derived by dividing every phasor in the vector diagram by direct-axis synchronous reactance X_d and multiplying them with the armature voltage as shown in Figure 4.7. The figure so obtained, contains P and Q as the x-axis and y-axis respectively which then can be upgraded by implementing different constraints to obtain the Figure 2.6 [22].

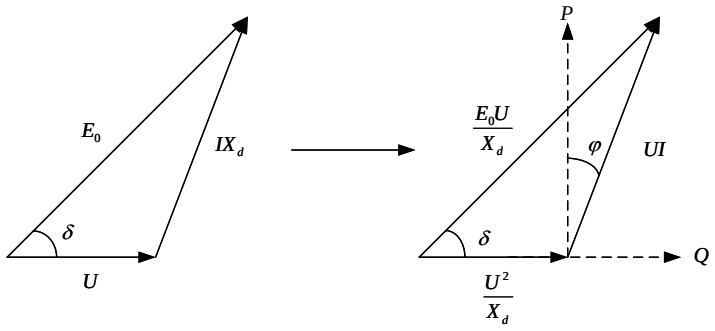

Figure 4.7: Derivation of a P-Q capability diagram from the phasor diagram (cylindrical rotor) [23].

In the On-line PQ diagram, all the defining parameters as mentioned before are achieved directly from the process and the point of operation is continuously updated in real time [22]. The parameters like active and reactive powers, terminal voltage, field current, frequency of grid, temperature and pressure of the cooling agent, varies during the operation so that the PQ diagram changes its configuration in real time. But the P, Q coordinate axes, and some curves like maximum and minimum turbine power and minimum field current do not changes. Temperature control system or the temperature of cooling agent (hydrogen, water) has a significant effect on the position of some operational limits like overheating limit of stator core end region, rated field current and the stator current limit [22].

Figure 4.8 shows the On-line PQ diagram with different operating conditions as follows:

- (1)- rated operation condition: voltage (U_n), frequency (f_n), hydrogen cooling gas temperature ($t_{\mathrm{n\ H2}}$).
- (2)- reduced terminal voltage $0.95U_n$.

- (3)-increased cooling gas temperature 1.1 $t_{\mathrm{n\ H2}}$.
- (4)- increased stator cooling water temperature 1.1 $t_{\mathrm{n\ water}}$ due to congested hollow copper strands.

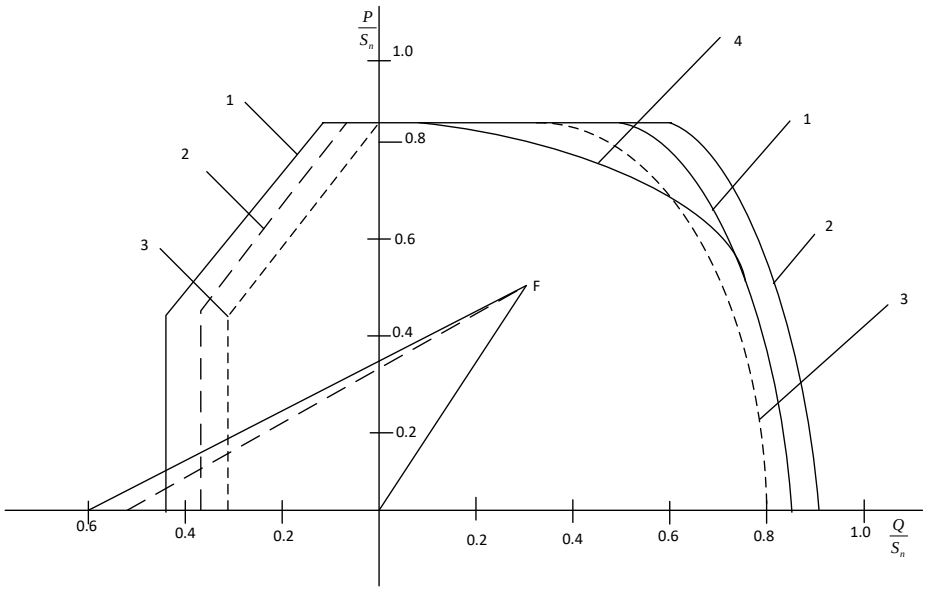

Figure 4.8: On-line PQ diagram with different operational condition from (1) -(4) [22].

4.3.1 Implementation of PQ diagram

The generator's capability diagram with different constraints as stated in Section 2.2 was implemented in MATLAB software environment. The MATLAB code used during the implementation of PQ diagram using visualization tool is provided in Appendix C. This software environment provides a sophisticated visualization for the implemented mathematical model of capability diagram. This thesis work presents the methodology for obtaining the PQ diagram for a cylindrical rotor synchronous generator with the following simplification during its modelling:

- The synchronous generator has been assumed to be connected to the infinite bus i.e. with constant voltage.
- The machine saturation effect on the direct axis synchronous reactance has not been considered, i.e. $X_d = \text{constant}$.
- The effect of armature resistance has been neglected.

The limits of the capability diagram which are implemented during its construction are as follows:

1. Rated turbine power limit
2. Rated stator Current limit
3. Rated field current limit
4. Practical stability limit

The rated parameters of generator G3 in local area in the 10-bus system is taken as reference for determining capability diagram which are as follows:

1. Rated terminal voltage, V: 13.8 kV
2. Rated MVA, S_n: 1600 MVA
3. Rated power factor, $\cos\phi_n$: 0.72 p.u.
4. Direct axis synchronous reactance, x_d: 2.07 p.u.
5. Stability margin: 10 %

Rated turbine power limit

The maximum and the minimum turbine power limits are drawn according to the following two conditions [24]:

- If the power of the turbine (P_T) exceeds the rated power of the generator (P_n), i.e. if $P_T > P_n$, then $P_{max} = P_n$.
- If the power of the turbine is equal to or less than the rated power of the generator ($P_T \leq P_n$), then $P_{max} = P_T.\eta_G$.

This limit is shown in Figure 4.9 labelled as P_{max}. The minimum power depends upon the turbine requirements. For example, in Kaplan and Francis turbine minimum power output is 5 % to 30% of rated output whereas in some turbines like Pelton turbine this limitation does not exists [24].

Rated stator current limit

The rated stator current limit is plotted as a constant semi-circle with center at origin '0' and radius as the rated apparent power, S_n as shown in Figure 4.9. Point 'P' denotes the rated operating condition of the generator which is defined at its rated power factor $cos\phi_n = 0.72$. So,
$P_{rated} = S_n cos\phi = 1 * 0.72 = 0.72$ p.u.
$Q_{rated} = S_n sin\phi = 1 * \sqrt{1 - (cos\phi)^2} = 0.69$ p.u.

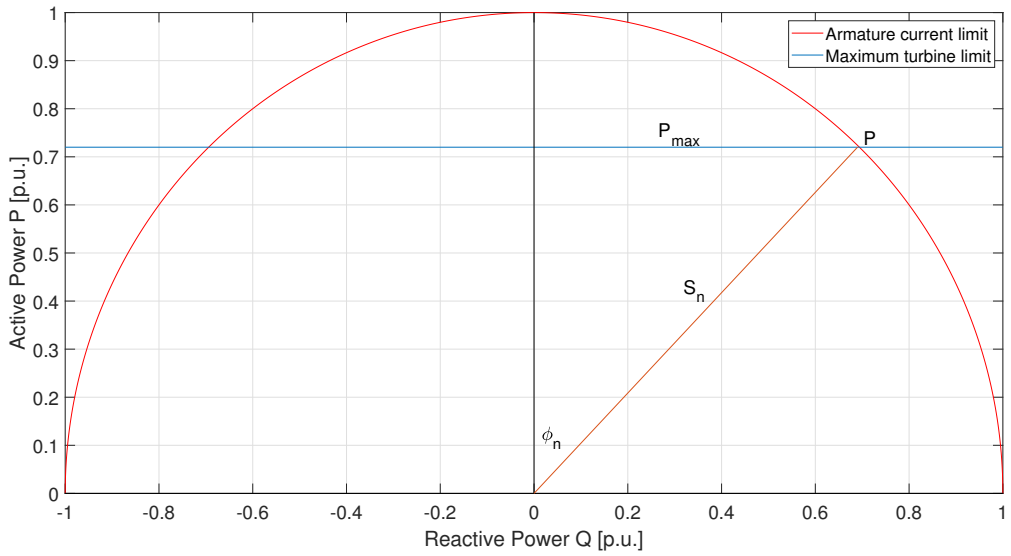

Figure 4.9: Rated stator current limit and maximum turbine limit plot.

Rated field current limit

The mathematical model for describing the field current limit has already been described in Section 2.2 by equation 2.11. Thus, an arc is drawn with the center at (0,-$\frac{V^2}{x_d}$) and radius $\frac{E_{qmax}V}{x_d}$ from $cos\phi = 0$ to $cos\phi = 0.72$ (rated) where E_{qmax} is calculated from the phasor diagram as shown in Figure 4.7 as:

$$E_{qmax} = \sqrt{(V + Ix_d sin\phi)^2 + (Ix_d cos\phi)^2}\ \text{p.u.} \tag{4.7}$$

The limit is drawn as curve PK in Figure 4.10.

Practical stability limit

For round-rotor generators, theoretical stability limit is achieved at load angle δ=90°. However, the theoretical stability curve is reduced by a constant power value, for example by 10% of the rating of the machine as a safety margin and the corresponding curve so obtained is termed as practical stability margin [15].

The theoretical stability curve is drawn as a straight line at point (0,-$\frac{V^2}{x_d}$)= (0,-$\frac{1}{2.07}$)= (0,-0.48) represented by dashed line in Figure 4.11. The practical stability limit is represented as curve AD in the same figure.

Hence, the safe region for the operation of a synchronous generator is represented by the area bounded by curve APKD in Figure 4.11.

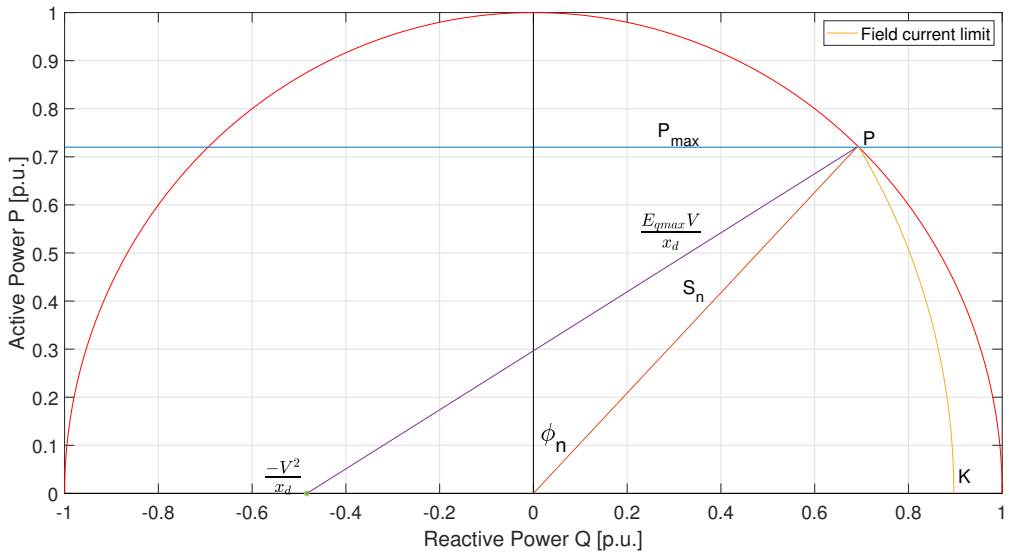

Figure 4.10: Rated field current limit plot.

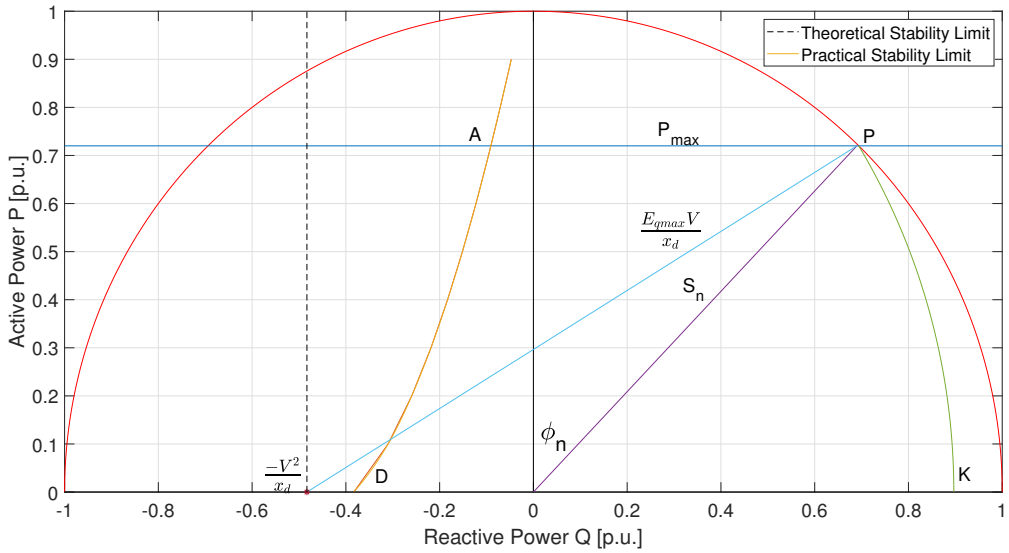

Figure 4.11: Theoretical and practical stability limit plot.

4.3.2 Automatic visualization tool for generator's capability

In Section 4.3.1, implementation of various operational limits in PQ diagram using MATLAB software environment was discussed. For improved visualization of the diagram, a visual App was created using MATLAB App designer. A Graphical User Interface was created by using different components from the component library and specifying app's

design and layout. For defining the App behavior, App designer allows an integrated version of the MATLAB Editor [25]. All the parameter values implemented, and the dynamics observed in the visualization tool is based upon the case study of Kundur 10-bus test system described in Section 4.2. Figure 4.12 shows a simple workflow diagram adopted during the implementation of generator's capability diagram in the visualization tool.

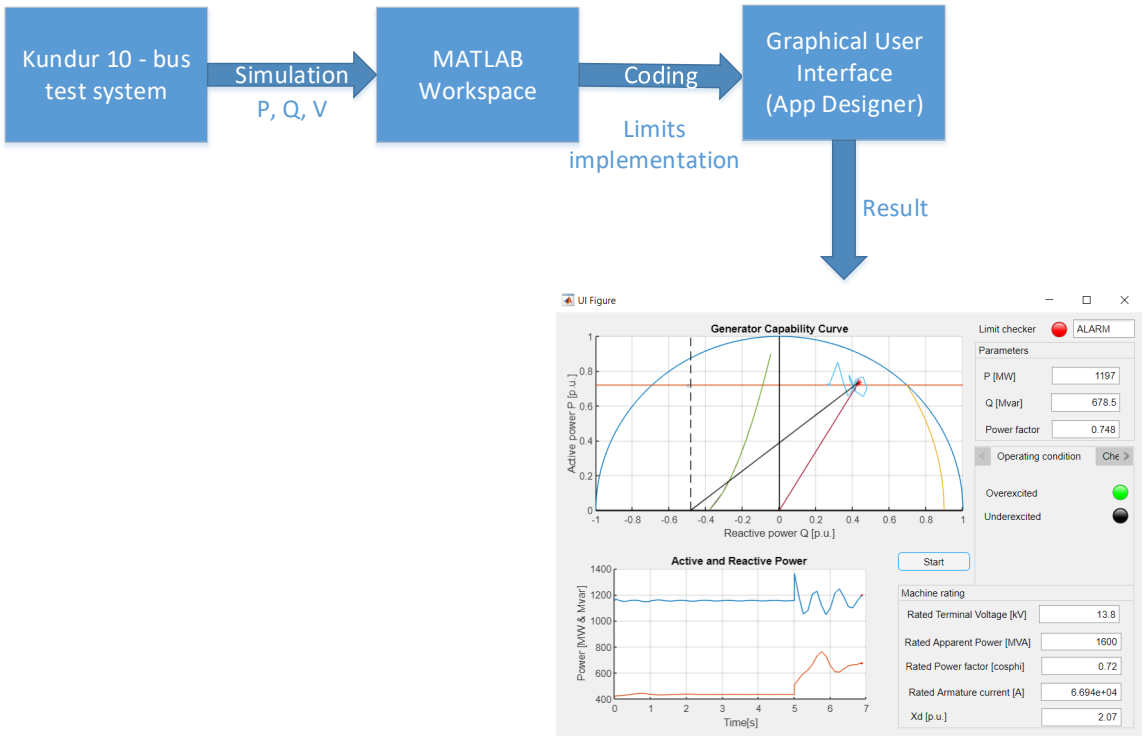

Figure 4.12: Work flow diagram for PQ curve implementation in visualization tool.

Figure 4.13 shows a GUI environment for the designed App in order to visualize the generator capability. The GUI consists of two figure windows and three tabs. The upper figure window (1) in the user interface shows the capability curve with the real-time operating point as indicated by 'red' asterisk symbol. The 'Parameters' tab (2) shows the operating point (P and Q) values in real time along with the operational power factor. Moreover, the dynamics of $\boldsymbol{P}$ and $\boldsymbol{Q}$ can be observed in the lower figure window (7). The 'Operating conditions' tab (3) shows the actual operating condition i.e. whether the generator is operating in over excitation mode or under excitation mode with current operation mode indicated by lamp glowing 'green'. The 'Machine rating' tab (4) indicates the generator rated conditions which can be changed by changing the values in the respective fields. For example, the effect of change of direct axis synchronous reactance on the generator limits can be visualized in the figure section (1) by changing its value in the 'Machine rating'

tab.

On top of the 'Parameters' tab resides a 'Limit checker' (5) as indicated by a lamp which glows 'red' when the defined operational limits on the capability curve are violated along with the actuation and information of 'ALARM' (6) to notify the operating personnel about the limit violation as shown in Figure 4.13. The lamp glows 'green' along with an information 'NORMAL' when the operating point lies within the defined boundaries as shown in Figure 4.14.

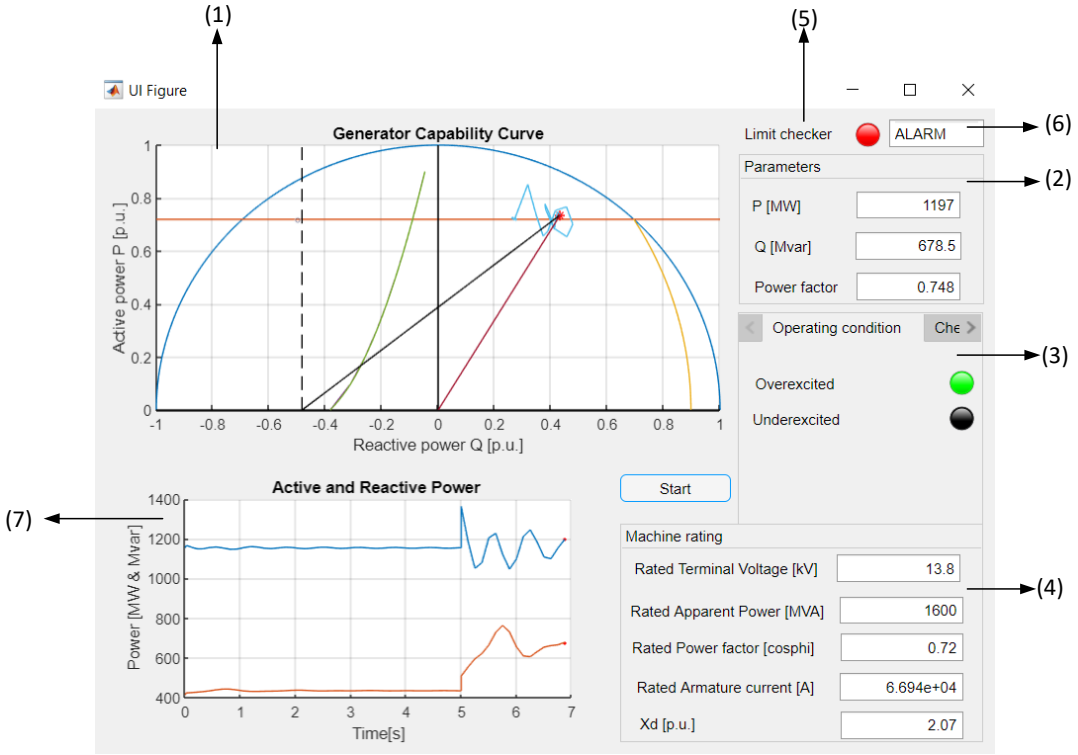

Figure 4.13: Graphical User Interface for Generator Capability Diagram.

4.3.3 Temperature visualization

This section demonstrates the visualization of temperature development in the rotor and stator winding of the synchronous machine in the same automatic visualization tool described in Section 4.3.2. Figure 4.15 shows the workflow process that was followed during temperature visualization. For the temperature observation, the local generator G3 in the test system was replaced by the 103 MVA hydrogenerator situated at 'Åbjøra' in Norway. The field current data I_{fd} and the terminal current data I_t obtained from the simulation is provided as MATLAB script in Appendix C.

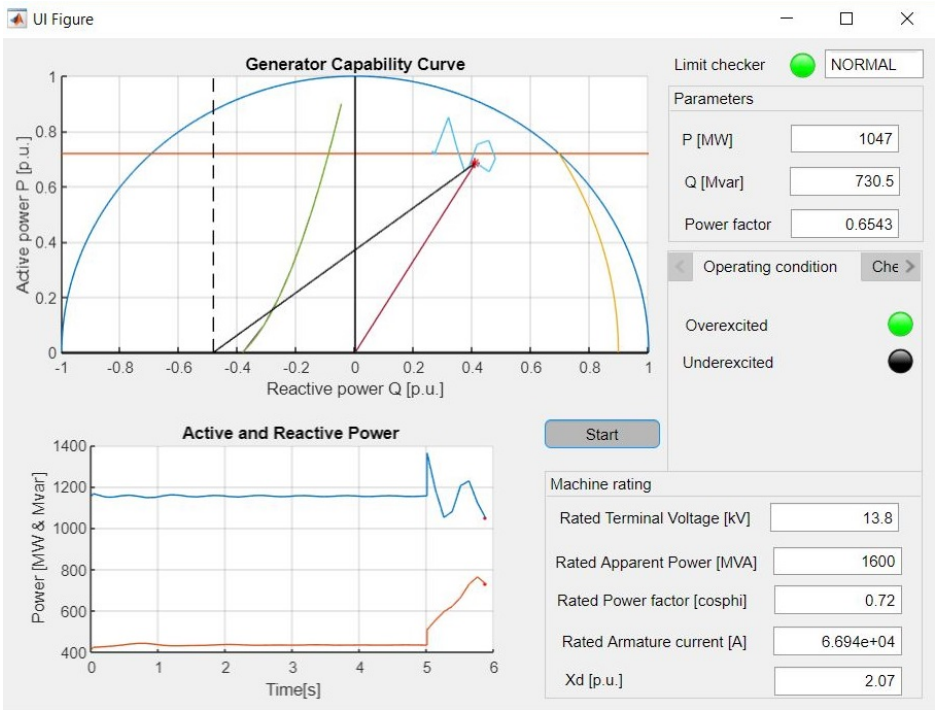

Figure 4.14: Graphical User Interface for Generator Capability Diagram showing 'NORMAL' condition.

Figure 4.16 shows the thermal model of a hydrogenerator developed in Simulink software environment as proposed in paper [3]. The circuit parameters used in the simulation are provided in Table B.5. Figure 4.17 shows the schematic setup which takes field current I_{fd} and the terminal current I_t from the local generator G3 as inputs and calculates the winding losses as I_{fd}^2R and I_t^2R respectively. The outputs rotor temperature T_r and the stator temperature T_s was extracted into the MATLAB workspace and then plotted. The inputs to the thermal model were continuously updated in real time from the workspace. The gain block in the output converts the measured voltage signal into the equivalent temperature signal. This gain factor (1/2236) was calculated by comparing the value of output measured signal from the 'Simulink model' as implemented in this thesis work and from 'DAE-ODE model' of the same low order thermal model described in [26].

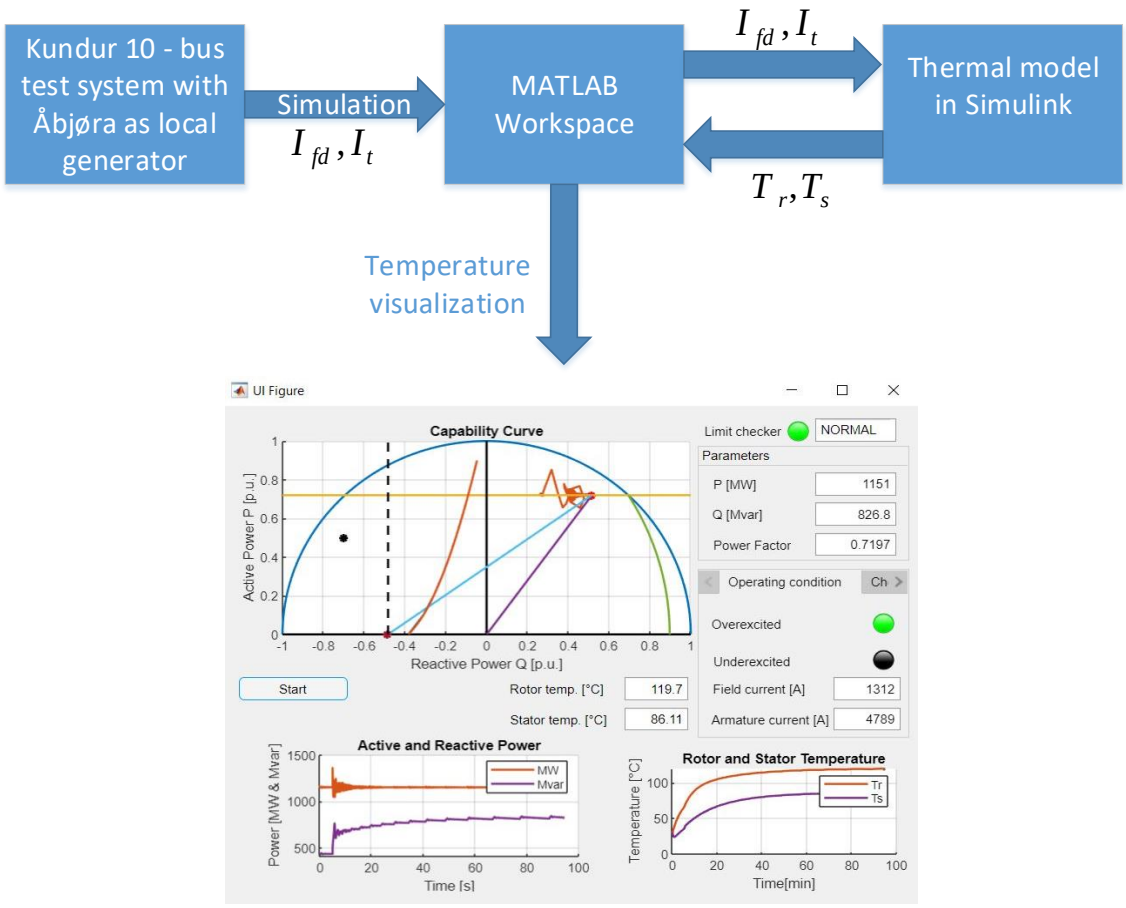

Figure 4.15: Work flow diagram for temperature visualization.

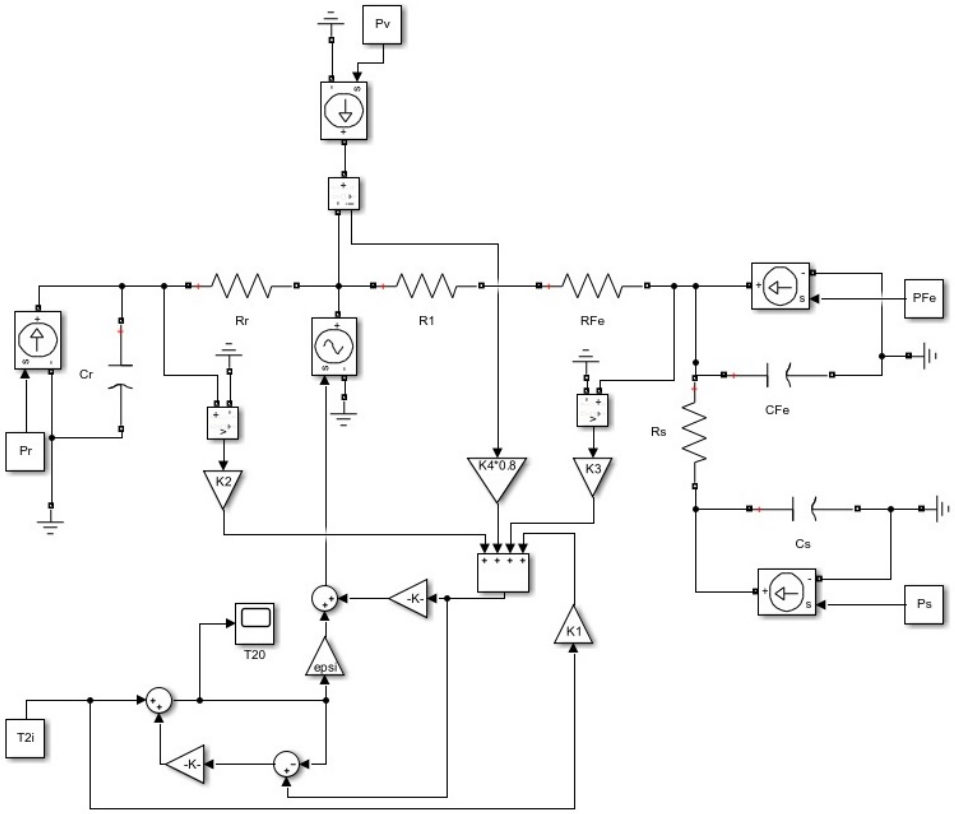

Figure 4.16: Simulink circuit for the thermal model proposed in [3].

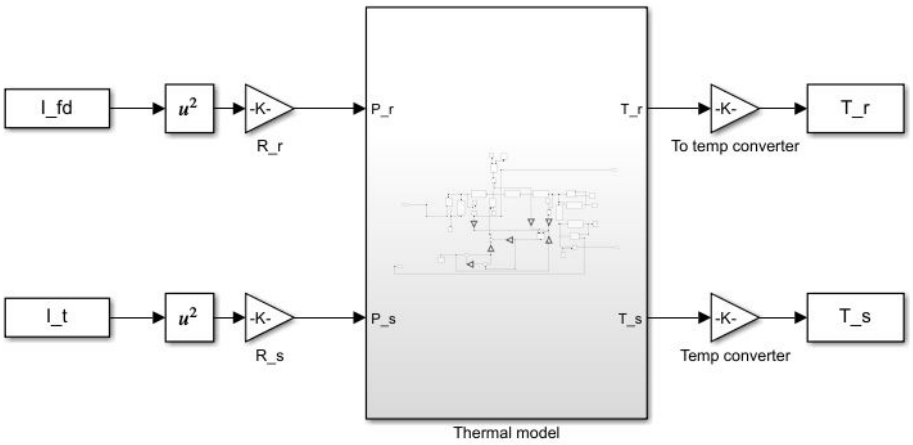

Figure 4.17: Schematic setup for the temperature measurement in Simulink [3].

5 Results and discussions

In this section, results and discussion regarding the simulation of 10-bus system and the PQ capability diagram has been presented.

Section 5.1 provides the results of load flow analysis of the test system. The effect of static load models and the influence of ULTC and OXL on long-term voltage stability is shown in this section. Furthermore, the outcome of the development of an automatic visualization tool is described in Section 5.2.

5.1 10-bus test system

Under the long-term voltage stability study, the impact of ULTC and OXL on voltage collapse was investigated. The voltage at various buses and the reactive power outputs of the generator was compared for the test system including and excluding the over excitation limiter with ULTC in action for both cases which are as presented in the Figures from 5.4 to 5.8. The steady state voltage profile and reactive power at different buses are shown in Figure 5.1 and 5.2 respectively.

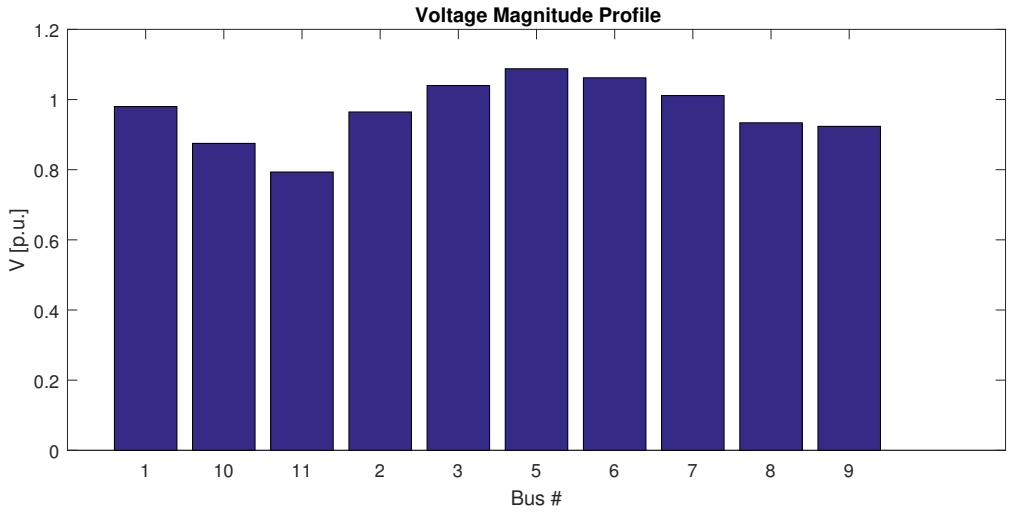

Figure 5.1: Steady state voltage at various buses.

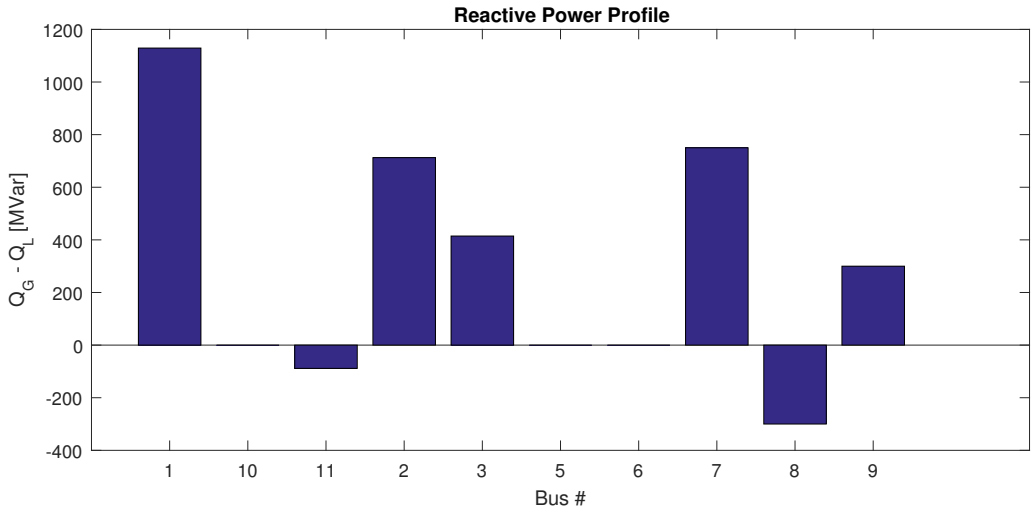

Figure 5.2: Steady state reactive power at various buses.

Four different cases were considered for the test system which is presented in Table 5.1. These cases are taken from the cases considered in dissertation [10] where the dynamic phenomenon was observed using PSS/E software taking the standard BPA power system.

Table 5.1: Case studies

Case	Load		OEL		ULTC
	Bus 8	Bus 11	G2	G3	
A	Constant impedance	Constant impedance	Inactive	Inactive	Inactive
B	Constant current	Constant impedance	Inactive	Inactive	Inactive
C	Constant power	Constant impedance	Inactive	Inactive	Inactive
D	Constant power	Constant impedance	Inactive	Active	Active
Scenario	Loss of transmission line between Bus 6 & Bus 7				

5.1.1 Effect of load models

As mentioned earlier in Chapter 3.1 about the types of load models, the effect of static load models on long term voltage stability was studied for the test case considered. Figure 5.3 shows the voltage profile at bus 11 under three cases namely A, B and C as presented in Table 5.1. For all these three cases, transformer T6 is equipped with a fixed tap ratio (instead of ULTC) of value equal to that of T5. Hence, the steady voltage at bus 11 before contingency in this case (0.814 p.u.) is different to the voltage magnitude (0.791 p.u.) as shown in Figure 5.4 where T6 is equipped with a ULTC.

From the voltage profiles in all three cases, it can also be seen that after the fault, the system stabilizes at lower voltages. The reason behind this is the inadequacy of reactive power in the system due to the disturbance considered. Due to tripping of one of the transmission line, the equivalent impedance of the line increases and hence the losses increases. In addition, the constant power load stabilizes at a lower value as compared to constant impedance and constant power load because of its load restoring characteristics [10]. That means constant power load tries to consume the same power at a pre-disturbance level as consumed power is independent of voltage variations and hence the voltage drops even further. The dynamics of voltage profile obtained is comparable to the similar case study performed in [10] using PSS/E software.

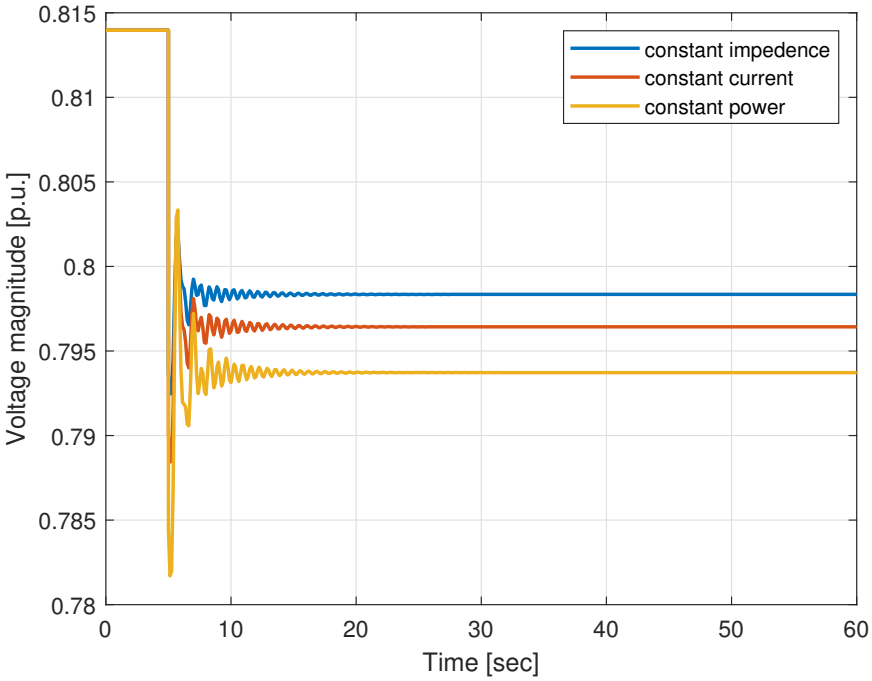

Figure 5.3: Voltage profile at bus 11 for different load types.

5.1.2 Effect of ULTC and OXL

In order to study the dynamics of ULTC and OXL in long term voltage stability scenario, Case D as mentioned in Table 5.1 was considered. The sequence of events triggered during the simulation in different time frames can be explained as follows.

- One of the transmission lines is disconnected at time t=5 seconds. When the line has been disconnected, the apparent impedance and consequently the line losses and voltage drop of the transmission system is increased.

- The second time frame starts at around 10 seconds where the ULTC is activated as the voltage at the bus 11 is lower than the preset value. The ULTC tries to keep the voltage at the secondary bus (bus-11) at its original value by adjusting its tap ratio which demands more reactive power support from the generators present in the network. Thus, to meet the increased reactive power demand the excitation current is continuously increased until the maximum tap of transformer is reached or voltages at the buses are recovered. This time frame can be observed in figures from 5.4a-5.8a. The voltage at bus 11 is restored to nearly its reference value in about 90 seconds as shown in Figure 5.4.
- The third time frame begins with the actuation of overexcitation limiter as shown in Figure 5.4b at around t=150 seconds by ramping down the field current. The following chains of events occurs after the actuation of OXL:
  - As the field current of G3 is reduced, its terminal voltage drops.
  - Voltages at bus 11, 10 and 7 drops.
  - ULTC on T6 tries to restore the voltage at bus 11 back to its original value.
  - The reactive power demand on generators increases. Field current of machine 3 increases and continues to remain at its limit and the terminal voltage of G3 further decreases.
  - Voltage at bus 7 drops and causes a further reduction in terminal voltage of bus 10 and bus 11.
  - The ULTC operates again, repeating above mentioned chains of events.

  Hence in response to each tap movement of ULTC, the voltage at bus 11 reduces rather than increased. This indicates that the system has entered into the voltage instability phase. The bus 11 voltage falls progressively as shown in Figure 5.4b until the ULTC reaches its maximum tap position at around 260 seconds. The voltage at bus 11 settles at around 0.77162 p.u.

5.1.3 Countermeasures against voltage collapse

There are different methods of mitigating voltage instability and preventing the power system from voltage collapse situation. Some of the preventive and corrective control for voltage stability based on paper [27] are as follows:

- Rescheduling of active power generation
- Implementation of generator secondary voltage control
- Additional shunt capacitance inclusion

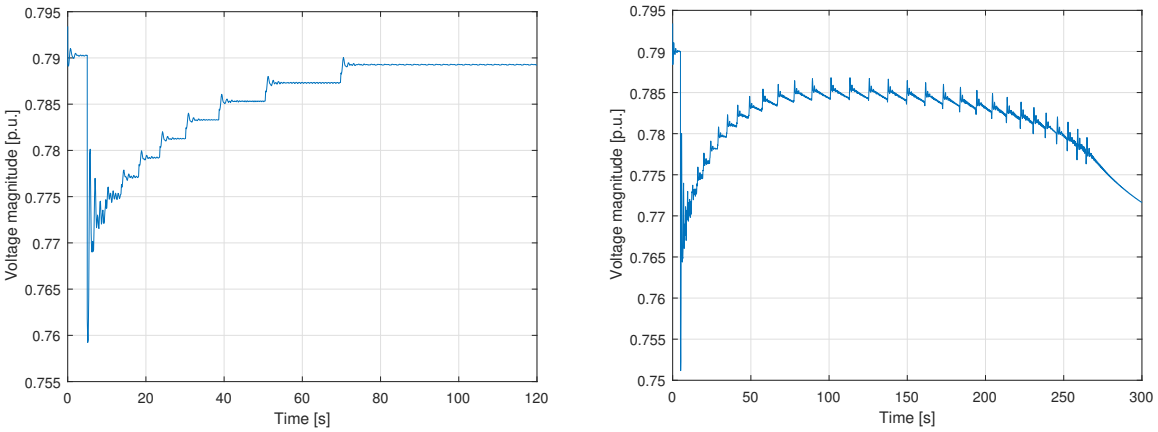

(a) With only ULTC (b) With ULTC and OXL

Figure 5.4: Bus 11 voltage without and with OXL.

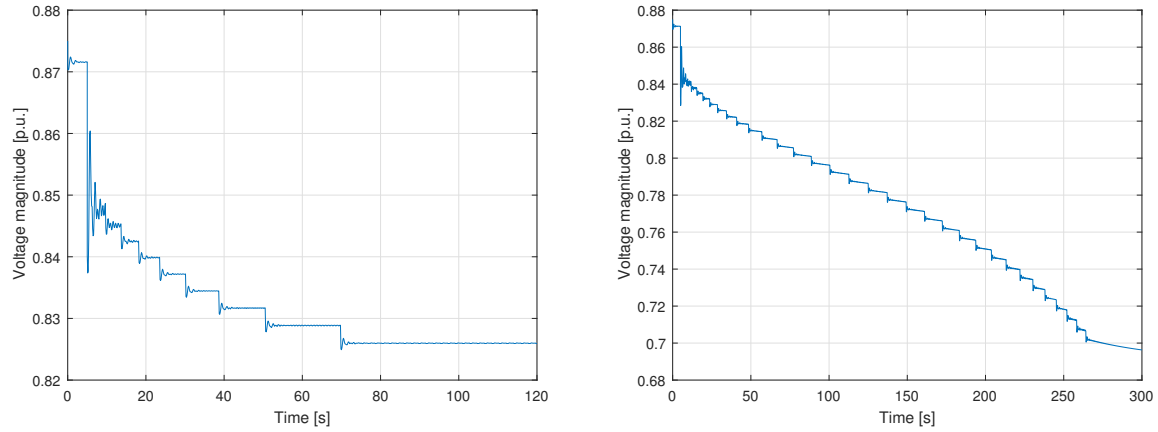

(a) With only ULTC (b) With ULTC and OXL

Figure 5.5: Bus 10 voltage without and with OXL.

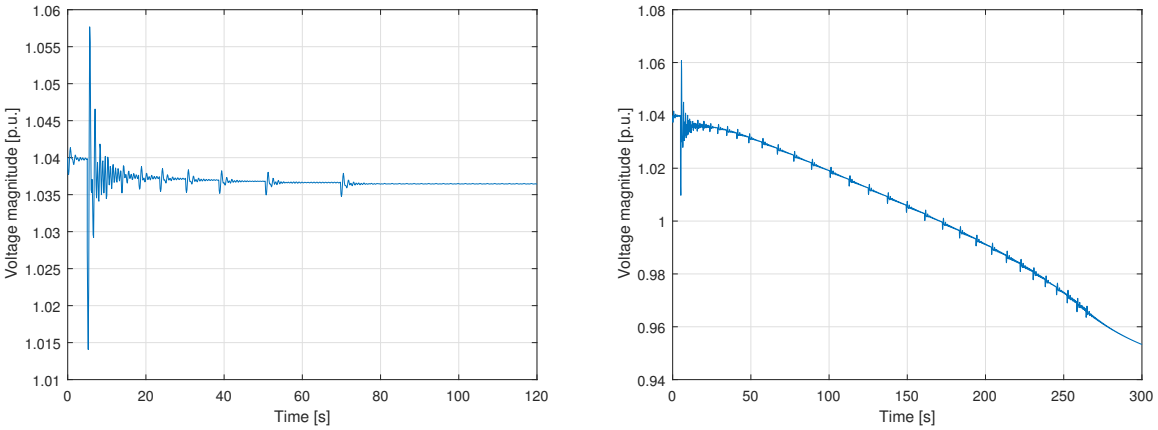

(a) With only ULTC (b) With ULTC and OXL

Figure 5.6: Bus 3 voltage without and with OXL.

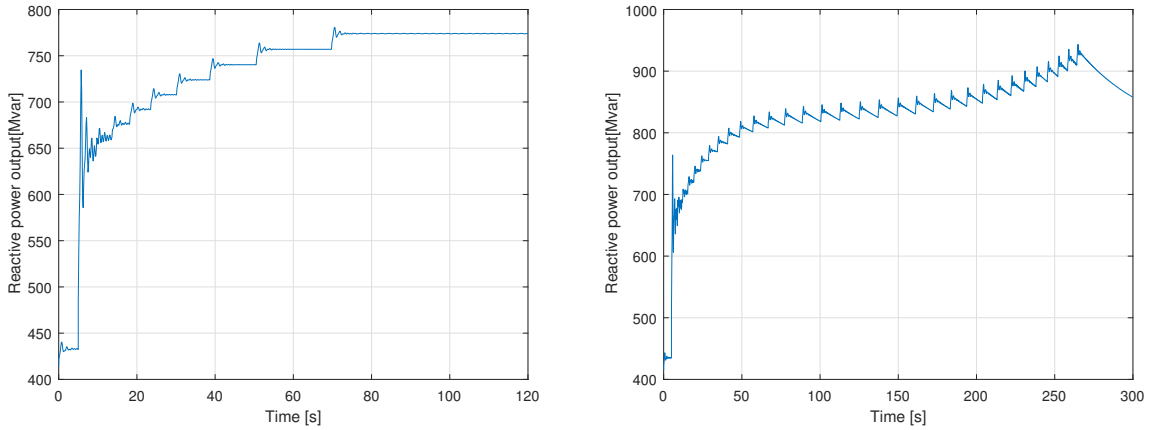

(a) With only ULTC (b) With ULTC and OXL

Figure 5.7: Reactive power output of generator G3 without and with OXL.

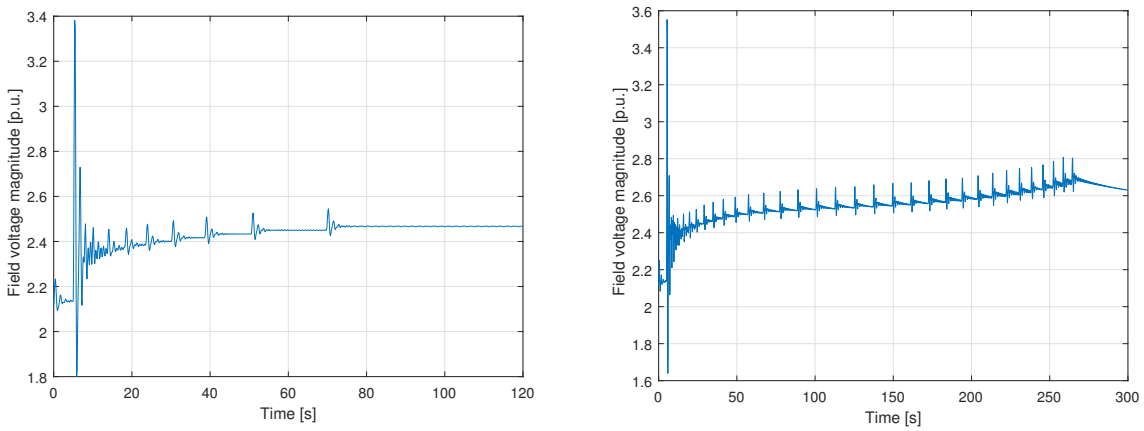

(a) With only ULTCL

(b) With ULTC and OXL

Figure 5.8: Field voltage at generator 3 without and with OXL.

- Adjustment of ULTC transformer taps; tap locking, tap blocking or tap reversing [10]
- Shedding of loads

The preventive and corrective control is an optimization problem where the objective function could be either minimizing the number of control equipment, load shedding minimization or the control cost minimization [27]. The issues and concepts regarding under-voltage load shedding which has been described as an economical solution to deal with voltage stability problem has been described in paper [6].

There was a combined influence of ULTC and current limiter of Generator G3 in voltage collapse of Kundur test system. Any of the above-mentioned control measures can be used as a mitigating measure for instability. The effect of load shedding and tap changer locking on the stabilization of voltages in the BPA test system is described by Larsson in [28].

5.2 Visualization tool for generator's capability

As mentioned in Section 4.3.2, an automatic visualization tool was developed in MATLAB software environment with GUI which provides real-time power factor, active and the reactive power. The generator reactive power capability can be visualized in a real-time along with an alarm signal in the case of limit violation.

In addition to the features described in Section 4.3.2, a 'Check condition' tab was implemented in the tool in order to confirm the indication of generators operation in both

over and under excited regimes. This operation is indicated by a black 'asterisk' as shown in Figure 5.9. User can give the active and the reactive power values as inputs in the 'Check condition' tab fields and the corresponding operation can be observed in both the capability chart and the lamp in the same tab which glows 'green' depending on whether the generator is over-excited or under-excited. For example, when the user gives a value of 0.5 and -0.7 in the P and Q fields, the operation will be observed as under excited indicated by 'under excited lamp' glowing 'green' as shown in Figure 5.10.

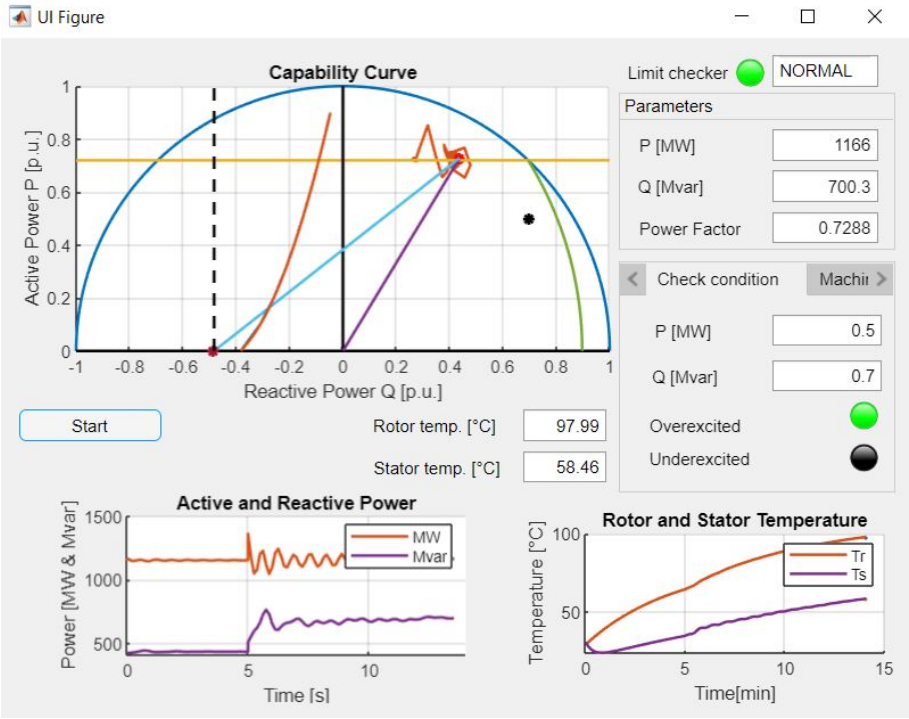

Figure 5.9: Visualization of generator operating point in over excited regime indicated by black asterisk.

The temperature development in the stator and rotor windings in the synchronous generator was also observed in the same tool which is as shown in Figure 5.11 and 5.12 using the thermal model as described in Section 3.3. The output temperatures as seen in the figure is the result of input field current and armature current taken from the local generator G3 in Kundur 10-bus system when replaced by 103 MVA hydrogenerator at 'Åbjøra' in Norway. The machine data of hydrogenerator is provided in Table B.6. The field and the stator currents in real time are observable in the tool. The initial temperature in the stator and rotor was taken as 28°C during the simulation. From Figure 5.12, it can be observed that the dynamics of temperature development is similar to the dynamics of the reactive power as seen in Figure 5.7b.

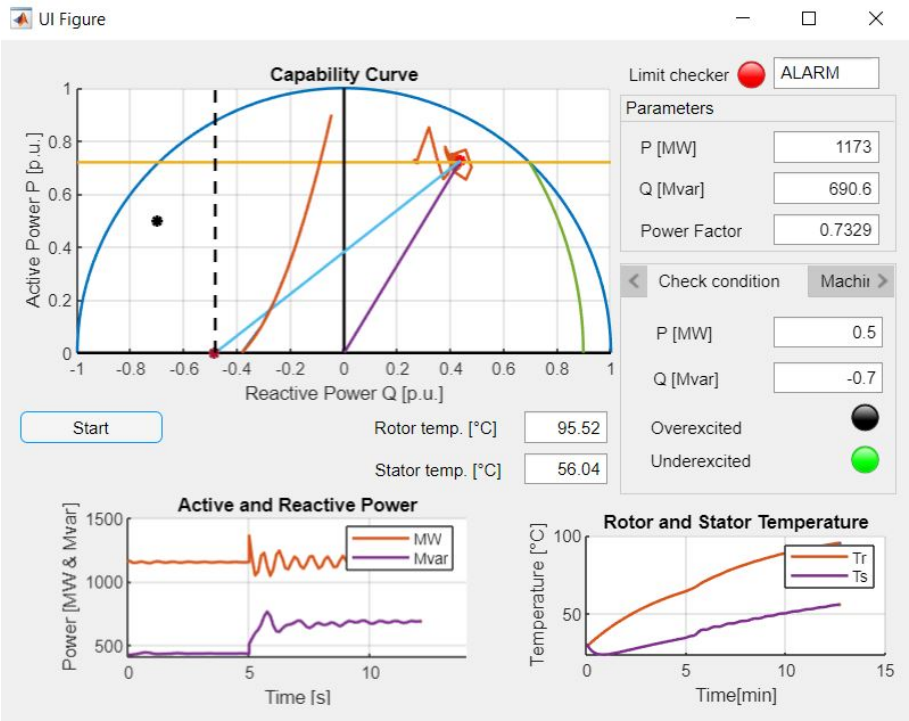

Figure 5.10: Visualization of generator operating point in under excited regime indicated by black asterisk.

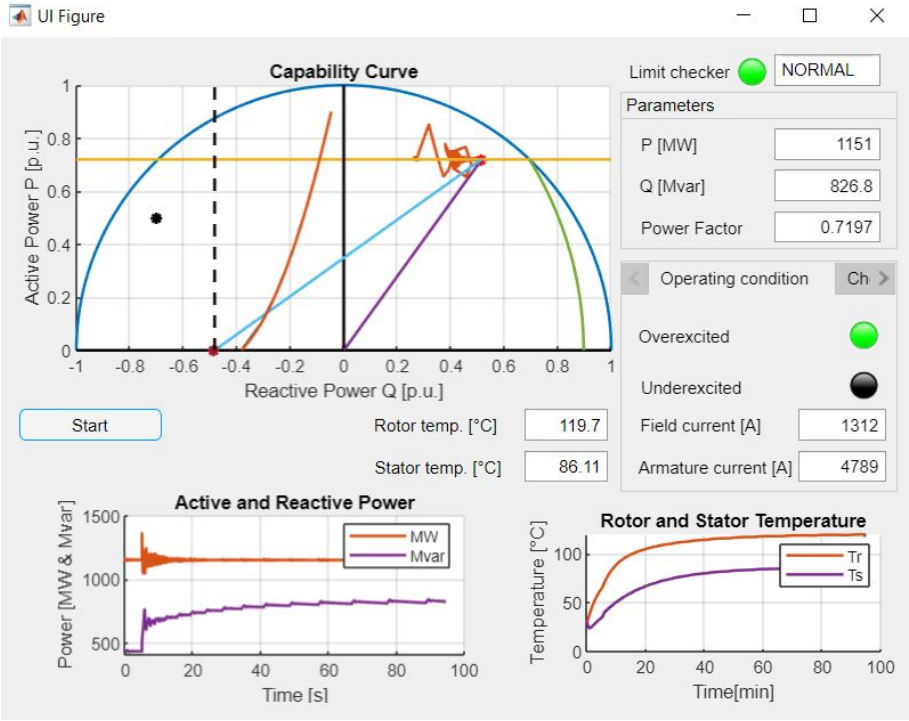

Figure 5.11: Temperature observation in the visualization tool.

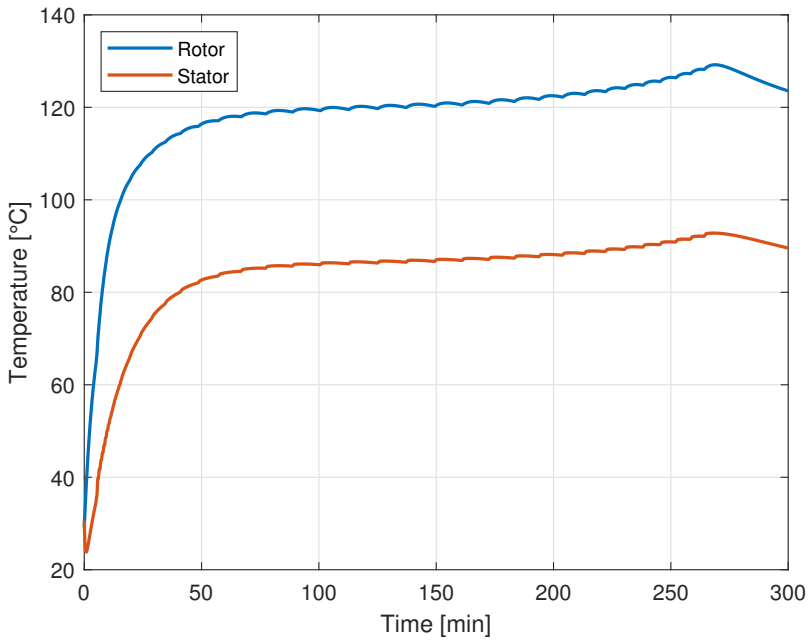

Figure 5.12: Rotor and Stator temperature plots from machine data 'Åbjøra'.

6 Conclusion

The dynamic analysis of voltage stability using time-domain simulation has been presented in this thesis work using a test power system containing 10 buses as a case study. From the simulation, it can be concluded that dynamic analysis is very useful in understanding the detail dynamics involved during the larger disturbances such as a loss of transmission line or loss of generation in the system and to study the coordination between the control and the protection as well. This type of analysis gives accurate results though it requires detail accurate models of the components and is time-consuming. A MATLAB based tool, PSAT was chosen as a long-term time domain simulation program where dynamic voltage stability was carried out and experienced to be little time consuming.

The influence of static load models on the voltage collapse scenario was presented. The severity of the effect depends upon the type of load. Constant power load has the most severe effect on the voltage collapse as compared to constant impedance and the constant current load. It is because the constant power loads are independent of the voltage and when the voltage drops in the network due to disturbances in the network, they try to consume the same power as pre-fault power so that the voltage drops even further. But the constant impedance loads decreases proportionally to the square of the voltage magnitude so has least effect on the voltage collapse.

Through long-term dynamic simulation, the dynamic behaviour of these two important power system components: ULTC and OXL is found to have huge influence on the voltage collapse phenomena. Accurate and detail modelling of these devices is necessary for detail and proper analysis of voltage stability.

The development and implementation of PQ capability diagram for the cylindrical rotor machine was done in MATLAB. The use of Graphical User Interface provides the user interaction with the visualization tool through graphical displays, inputs and visual indicators. During implementation, the infinite bus-bar assumption was made which is not practical in real case as the terminal voltage can significantly vary from the rated value. As the terminal voltage varies, the field and the armature limits also vary. Furthermore, the assumption of constant direct-axis synchronous reactance is also not valid as the synchronous machine are designed with certain amount of saturation level and depends upon machine operating point such as armature voltage and current [23].

While implementing the Åbjøra hydrogenerator as a local generator (G3) in the test power system considered, it was found that the OXL does not came into the operation

as expected. The reason could be the inappropriate parameters for the load flow analysis as every parameter values for the models were scaled down for this comparatively lower rating hydrogenerator during implementation. An already developed thermal model in [2] was used to visualize the temperature of hydrogenerator in the visualization tool.

7 Further work

Some of the recommendations which can be undertaken as a further work are presented below.

- This thesis work presented the effect of generator overexcitation limiter, transformer tap changer and the static loads on the voltage stability. The effect of dynamic load characteristics which has a significant influence on voltage stability can be analyzed further. Moreover, other simulation tools like PSS/E, DIgSILENT PowerFactory, EUROSTAG, SimPowerSystems, EPRI Extended Transient Mid-Term Stability Program (ETMSP) can be used to test and compare results from the same test system for voltage instability and collapse phenomena.
- The generator PQ capability diagram was implemented in this thesis assuming cylindrical rotor machine. Salient pole generators on the other hand exhibit different characteristics in the under-excited regime. The theoretical and practical stability limit curve for salient pole machine is different to that of cylindrical rotor machine as it contains both the direct and quadrature axis reactances as seen in Figure 2.6. Furthermore the minimum rotor field current limit is present only in salient pole machines due to additional reluctance power in such machines [9]. Hence, both types of aforementioned limits could be executed in PQ diagram for salient pole machine. Moreover, the stator end region heating limit which imposes an additional limit in under-excited region of generator capability diagram can also be analyzed under the further work.
- Change of generator terminal voltage changes the boundaries defined in capability diagram. In this thesis work, the limits are defined taking the generator terminal voltage as 1 p.u. So, the effect of change of terminal voltage on the PQ capability limits can be analyzed further. Moreover, the dependency of apparent power on other factors such as inlet air temperature of a cooling system, maximum tension of the coupled rotor on fault conditions, capacity of a cooling system could be studied while defining the armature current limit [29].

Bibliography

[1] CIGRE Task Force 38.02.10, 'Modelling of Voltage Collapse Including Dynamic Phenomena', Tech. Rep., 1993.

[2] T. Øyvang, 'Enhanced power capability of generator units for increased operational security', PhD thesis, 2018.

[3] T. Øyvang, J. K. Noland, G. J. Hegglid and B. Lie, 'Online model-based thermal prediction for flexible control of an air-cooled hydrogenerator', *IEEE Transactions on Industrial Electronics*, pp. 1–1, 2018. DOI: 10.1109/tie.2018.2875637.

[4] P. Kundur, *Power System Stability and Control*. McGraw-Hill, Inc., 1994.

[5] 'Definition and classification of power system stability IEEE/CIGRE joint task force on stability terms and definitions', *IEEE Transactions on Power Systems*, vol. 19, no. 3, pp. 1387–1401, Aug. 2004. DOI: 10.1109/tpwrs.2004.825981.

[6] C.W.Taylor, 'Concepts of undervoltage load shedding for voltage stability', *IEEE Transactions on Power Delivery*, vol. 7, no. 2, pp. 480–488, Apr. 1992. DOI: 10.1109/61.127040.

[7] (2019). Voltage stability, [Online]. Available: http://shodhganga.inflibnet.ac.in/bitstream/10603/40792/7/07_chapter2.pdf (visited on 02/02/2019).

[8] D. Thukaram, L. Jenkins, H. Khincha, G. Yesuratnam and B. Kumar, 'Monitoring the effects of on-load tap changing transformers on voltage stability', in *2004 International Conference on Power System Technology, 2004. PowerCon 2004.*, IEEE. DOI: 10.1109/icpst.2004.1460031.

[9] V. Storvann, 'Maintaining voltage stability : An analysis of voltage stability indicators and mitigating actions', Master's thesis, Norwegian University of Science and Technology, 2012.

[10] D. T. Nguyen, 'Contributions to analysis and prevention of power system blackouts', Theses, Institut National Polytechnique de Grenoble - INPG, Nov. 2008. [Online]. Available: https://tel.archives-ouvertes.fr/tel-00352414.

[11] M. Hasani and M. Parniani, 'Method of combined static and dynamic analysis of voltage collapse in voltage stability assessment', in *2005 IEEE/PES Transmission & Distribution Conference & Exposition: Asia and Pacific*, IEEE. DOI: 10.1109/tdc.2005.1547182.

[12] J. Dragosavac, D. Arnautovic, Z. Janda, J. Milanovic and B. Radojicic, 'On-line estimation of available generator reactive power for network voltage support', in *8th Mediterranean Conference on Power Generation, Transmission, Distribution and Energy Conversion (MEDPOWER 2012)*, Institution of Engineering and Technology, 2012. DOI: 10.1049/cp.2012.2014.

[13] D. E. Moghadam, A. Shiri, S. Sadr and D. A. Khaburi, 'A practical method for calculation of over-excited region in the synchronous generator capability curves', in *2014 IEEE 23rd International Symposium on Industrial Electronics (ISIE)*, IEEE, Jun. 2014. DOI: 10.1109/isie.2014.6864702.

[14] J. Machowski, J. W. Bialek and J. R. Bumby, *Power System Dynamics : Stability and Control*, 2nd ed. John Wiley & Sons, Ltd, 2008.

[15] J. Walker, 'Operating characteristics of salient-pole machines', *Proceedings of the IEE - Part II: Power Engineering*, vol. 100, no. 73, pp. 13–24, Feb. 1953. DOI: 10.1049/pi-2.1953.0004.

[16] B. M. Weedy, B. J. Cory, N. Jenkins, J. B. Ekanayake and G. Strbac, *Electric Power Systems*, 5th ed. Wiley, 2012.

[17] C. W. Taylor, *Power System Voltage Stability*. McGraw-Hill, 1993.

[18] *IEEE standard for salient-pole 50 hz and 60 hz synchronous generators and generator/motors for hydraulic turbine applications rated 5 MVA and above*. DOI: 10.1109/ieeestd.2006.99082.

[19] C. Mejuto, 'Improved lumped parameter thermal modelling of synchronous generators', PhD thesis, 2010. [Online]. Available: https://www.era.lib.ed.ac.uk/handle/1842/4612.

[20] F. Milano, *Power System Analysis Toolbox Documentation for PSAT*, version 2.1.8, 2013.

[21] CIGRE Task Force 38.02.08, 'Long Term Dynamics Phase II', CIGRE, Tech. Rep., 1995.

[22] Working Group A1.38, 'Generator On-Line Over and Under Excitation Issues', Technical Brochure CIGRE, Jun. 2015.

[23] M. Vrazic, A. Viskovic and Z. Hanic, 'User P-Q Diagram as a Part of a Synchronous Generator Monitoring System', *Electronics and Electrical Engineering*, vol. 20, no. 4, Apr. 2014. DOI: 10.5755/j01.eee.20.4.5333.

[24] I.Ilić, Z. Maljković, I. Gašparac, M. Pavlica, D. Ilić-Zubović, V. Jarić, A. Višković and R. Belobrajić, 'Methodology for Determining the Actual PQ Diagram of a Hydrogenerator', *Journal of Energy*, vol. 56, no. 2, pp. 144–181, 2007. [Online]. Available: https://hrcak.srce.hr/13153.

[25] (2019). Matlab app designer, [Online]. Available: https://se.mathworks.com/products/matlab/app-designer.html (visited on 22/03/2019).

[26] M. Pandey, 'Model fitting and state estimation for thermal model of synchronous generator', unpublished thesis, 2019.

[27] V. A. Qin Wang, 'A critical review on preventive and corrective control against voltage collapse', *Electric Power Components and Systems*, vol. 29, no. 12, pp. 1133–1144, Dec. 2001. DOI: 10.1080/153250001753246862.

[28] M. Larsson, 'Coordinated voltage control in electric power systems', PhD thesis, 2000. [Online]. Available: http://www.iea.lth.se.

[29] D. E. Moghadam, A. Shiri, S. Sadr and D. A. Khaburi, 'A practical method for calculation of over-excited region in the synchronous generator capability curves', in *2014 IEEE 23rd International Symposium on Industrial Electronics (ISIE)*, IEEE, Jun. 2014. DOI: 10.1109/isie.2014.6864702.

[30] T. Øyvang, G. J. Hegglid and B. Lie, 'Models of synchronous generators with excitation system, for transient power system studies', *IFAC-PapersOnLine*, vol. 51, no. 2, pp. 91–96, 2018. DOI: 10.1016/j.ifacol.2018.03.016.

Appendix A

Signed version of task description

University of
South-Eastern Norway

Faculty of Technology, Natural Sciences and Maritime Sciences, Campus Porsgrunn

FMH606 Master's Thesis

Title: Online monitoring and visualizing of a generators capability with Simulink.

USN supervisor: Thomas Øyvang, co-supervisor Dietmar Winkler

External partner: Statkraft

Task background:

AC electrical power is produced by a synchronous generator driven by a turbine (prime mover) and is the primary source of active P and reactive Q power in the power system. The generated power (which is the product of voltage and current) is fed into the transmission network via a step-up transformer. The power factor cosϕ of an AC electrical power system is defined as the ratio of the real power flowing to the load, to the apparent power in the circuit. Generators normally provide the primary source of voltage and reactive power support during voltage emergencies. A power system undergoes voltage collapse if the post-disturbance voltages are outside of acceptable limits. Voltage collapse may be total (blackout) or partial. Longer-Term Voltage Stability involves a large disturbance,
and/or load change or power transfer change. Voltage collapse involves slow load restoration by tap changing and generator/condensers with limiters. The time frame
is usually 0.5 to 30 minutes. The reactive power is continuously adjustable under the control of a voltage regulator.

In a recent Ph.D. study (Øyvang, 2018), the possibility of modelling and controlling the thermal development in a synchronous generator was developed. To monitor the reactive power output of generators and operate them to keep appropriate reactive power reserve at generators at all time is one of the most important countermeasure for voltage collapse. This task contains the development and implementation of the PQ capability diagram for online monitoring and control in Simulink. The approach and methodology can be used for the implementation of the user real-time P-Q diagram whose limits change dynamically in accordance with operating conditions when the generator operates on the grid. This enables better insight into the operational limits which ensures better utilization of the synchronous generator.

References:

Øyvang, Thomas (2018). *Enhanced power capability of generator units for increased operational security*. Ph.d.-thesis, University of South-Eastern Norway.

Kundur, Prabha (1994). Power System Stability and Control, Mc graw hill.

Task description:

This thesis will contain different issues regarding:

- Survey on the voltage stability and collapse phenomena.
- Survey on a generators capability and how it operates.

Address: Kjølnes ring 56, NO-3918 Porsgrunn, Norway. **Phone:** 35 57 50 00. **Fax:** 35 55 75 47.

- Develop a simulation model of the Kundur's 10 bus system (Kundur, 1994) and do long term voltage stability analysis of the system preferably on the dynamics of the On-Load Tap Changer (OLTC) and the OverExcitation Limiter (OEL).
- The modelling shall be carried out in a Simulink environment tool e.g., such as PSAT and results should be verified to (Kundur, 1994). Make use of standard dynamic models and control system. Understand the different models involved.
- Develop an automatic visualization tool for a generators capability and implement it in the 10 bus system.
- If time allows, implement the hydrogenerator used in (Øyvang, 2018) as the "local" generator in the 10 bus system. In addition, an already developed thermal model of the machine will be given to the candidate. This can then be used to also visualize temperatures in the same visualization tool.
- The outcome of the study is intended to be suitable for a conference/journal paper, and the Master's Thesis shall be written in LaTeX. A suggestion for a preliminary paper should be put in the appendix. All developed models shall be handed in with the report. Present the thesis work.

Student category: EPE

Practical arrangements:

Supervision:

As a general rule, the student is entitled to 15-20 hours of supervision. This includes necessary time for the supervisor to prepare for supervision meetings (reading material to be discussed, etc).

Signatures:

Supervisor (date and signature): Thomas Øyvang

Student (write clearly in all capitalized letters): PRABESH KHADKA

Student (date and signature): 28/01/2019

Appendix B

Parameters used in the Kundur test system and the thermal model

B.1 System diagram

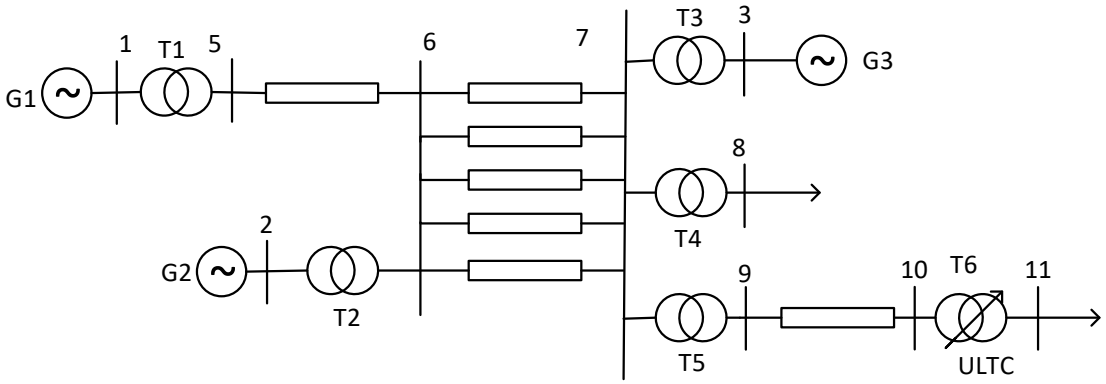

Figure B.1: Single line diagram of test system [21].

B.2 Load flow data

S_{base} = 100 MVA

Table B.1: Bus data of test system

Bus	**Base [kV]**	**Vscheduled [p.u.]**	**Phase [rad]**	**Shunt [Mvar]**	**P load [MW]**	**Q load [Mvar]**
Bus1	13.8	0.98	0	0	0	0
Bus2	13.8	0.96	0	0	0	0
Bus3	13.8	1.04	0	0	0	0
Bus5	500	1.00	0	0	0	0
Bus6	500	1.00	0	0	0	0
Bus7	500	1.00	0	750	0	0
Bus8	13.8	0.94	0	1500	3000	1800
Bus9	115	0.95	0	300	0	0
Bus10	115	0.89	0	0	30	0
Bus11	13.8	0.91	0	0	3100	90

Table B.2: Generators load flow data

Bus No.	**Gen Name**	**Base [kV]**	**P gen [MW]**	**Q gen [Mvar]**	**Sbase [MVA]**	**Qmax [Mvar]**	**Qmin [Mvar]**
1	G1	13.8	3471.9	1129.03	5000	1600	-1000
2	G2	13.8	1736	712.53	2200	725	200
3	G3	13.8	1154	414.58	1600	700	-100

Table B.3: Transmission lines data

From Bus	**To bus**	**R [p.u.]**	**X [p.u.]**	**B [p.u.]**
5	6	0.0000	0.0040	0.0000
6	7	0.0015	0.0288	1.1730
9	10	0.0010	0.0030	0.0000

Table B.4: Transformers data

Transformer	**R [p.u.]**	**X [p.u.]**	**Tap ratio**
T1	0.0000	0.0020	0.8857
T2	0.0000	0.0045	0.8857
T3	0.0000	0.0125	0.9024
T4	0.0000	0.0030	1.0664
T5	0.0000	0.0026	1.0800
T6	0.0000	0.0010	0.9750

B.3 Dynamic data

Machine parameters:

Machine 1: Infinite bus
Machine 2: H = 2.09, MVA rating = 2200 MVA
Machine 3: H= 2.33, MVA rating = 1400 MVA

Following are the parameters for machine 2 and machine 3 on their respective MVA

ratings:

$R_a = 0.0046$	$X_d = 2.07$	$X_q = 1.99$
$X_l = 0.155$	$X'_d = 0.28$	$X'_q = 0.49$
$X''_d = 0.215$	$X''_q = 0.215$	
$T'_{do} = 4.10$	$T'_{qo} = 0.56$	
$T''_{do} = 0.033$	$T''_{qo} = 0.062$	

Exciters:

Both machine 2 and machine 3 uses thyristor exciters with a gain of 100 and the time delay of the measurement system as 0.02 seconds.

Overexcitation limiter for machine 3:

The OXL model used in the simulation is as described in the Section 4.2.2 with integrator time constant (T_0)= 60 seconds, maximum field current $i_{fd}^{\mathbf{lim}}$= 11.7 p.u. and maximum output signal $v_{\mathbf{OXL}}^{\max}$= 5.02 p.u.

ULTC data for transformer T6 between bus 10 and 11:

Deadband: ±1% p.u. bus voltage
Tap range: ±16 steps
Step size: 5/8 % (=0.00625 p.u.)

B.4 Thermal model parameters

Table B.5: Thermal model data [3]

Parameters	Symbol	Value	Unit
Thermal resistance, $T_{Fe} - T_{\delta}$	R_{Fe}	0.07	K/kW
Thermal resistance, $T_s - T_{Fe}$	R_s	0.05	K/kW
Thermal resistance, air	R_1	0.018	K/kW
Gain coefficient, $T_{2,i}$	K1	0.59	-
Gain coefficient rotor(Cu)	K2	0.5	-
Gain coefficient stator(Fe)	K3	0.36	-
Heat exchanger effieicency (epsi)	ε	0.595	-

B.5 Machine data of Åbjøra

Table B.6: Machine data of Åbjøra [30]

Description	Parameters	Value	Unit
Rated power	S_n	103	MVA
Rated voltage	V_{tn}	11	kV
Rated current	I_{tn}	5406	A
Rated field current	I_{fdn}	1064	A
Inertia constant	H	2.66	s
Number of polepairs	p	6	-
Synchronous reactance d-axis	x_d	1.09	[p.u.]
Synchronous reactance q-axis	x_q	0.67	[p.u.]
Transient reactance d-axis	x'_d	0.24	[p.u.]
Subtransient reactance d-axis	x''_d	0.15	[p.u.]
Subtransient reactance q-axis	x''_q	0.19	[p.u.]
Transient OC Time constant d-axis	T'_{do}	10	s
Transient OC Time constant q-axis	T'_{qo}	0.23	s
Subtransient OC Time constant d-axis	T''_{do}	0.086	s
Subransient OC Time constant q-axis	T''_{qo}	0.23	s
Stator leakage inductance	X_l	0.08	[p.u.]
Stator resistance	R_a	0.00182	[p.u.]

Appendix C

Codes and programs used in the thesis work

The MATLAB code used for the development of visualization tool and the models developed can be access through the following GitHub link.

`https://github.com/prabesh213922/Thesis.git`

The suggestions for using those files is included in the 'README' file provided in the same folder.

Appendix D

Paper for SIMS conference

The preliminary version of the paper regarding the thesis work is provided in this section.

Online Monitoring and Visualizing of a Generator's Capability with Simulink

Prabesh Khadka Dietmar Winkler Thomas Øyvang

Department of Electrical Engineering, Information Technology and Cybernetics, University of South-Eastern Norway, Porsgrunn, Norway {versatile.prabesh}@gmail.com

Abstract

The power systems today are becoming more larger, complex and are operating closer to its security and stability limits particularly due to an increase in load demands and number of environmental concerns. Voltage stability has been a major subject of discussion and concern in electric power system operation and planning worldwide. This research paper presents the long-term voltage stability analysis of a power system using time-domain simulation with PSAT software. Furthermore, a mathematical approach of plotting PQ capability diagram of a generator is suggested in MATLAB software environment. It is shown that the load models, load tap changing transformer and generator over-excitation limiter have a significant influence on voltage stability and collapse phenomena.

Keywords: long-term voltage stability, dynamic voltage stability, generator capability diagram, PSAT (Power System Analysis Toolbox)

1 Introduction

Voltage instability is becoming one of the major issues in power system operation and planning worldwide due to the increased power demand. Many incidents of voltage collapse have been reported at different corners of the world and few examples can be found in CIGRE report (CIGRE Task Force 38.02.10 1993). The inability of the power system to meet the reactive power demand in an electrical network is one of the cause of voltage instability. Generators are normally the sources of reactive power support during voltage insecurities. So, monitoring the voltage profiles, voltage regulation and the reactive power output of generators is one of the important countermeasures for voltage collapse.

In a recent Ph.D. study (Øyvang 2018), utilization of the thermal capacity of a hydrogenerator to enhance the voltage stability of the power system was studied. The available voltage control capability depends upon the temperature rise of the machine during contingencies (Øyvang 2018). Furthermore, the normal limits of operation of generators without exceeding their thermal limitations is defined by the reactive capability curve. This paper will primarily address the implementation of PQ capability diagram for online monitoring of generators capability. In addition, long term voltage stability or the collapse phenomenon which includes the dynamics of slow acting components such as load tap changers, generator excitation limiters and thermostat controlled loads, has been investigated in this research work.

The dynamic simulation is carried out on Kundur 10-bus test system (Kundur 1994), in MATLAB based power system toolbox PSAT; a Free and Open Source Software (FOSS) which includes different static and dynamic power system component models. Moreover, the PQ capability diagram is implemented in the MATLAB programming language with the help of Graphical User Interface.

This paper is organized as follows. Section 2 gives a brief introduction to voltage stability and its types depending upon the time frame. Section 3 provides the description of the test system and the models of components used in the test system. The simulation results and the discussions regarding long-term voltage analysis are included in the same section. Section 4 presents the generator capability diagram whereas the description about the *visualization tool* is included in Section 5. Finally, Section 6 presents the conclusion and further work.

2 Voltage Stability

The ability of a power system to maintain the steady acceptable voltage at all the buses during normal operating conditions and after being subjected to the disturbance can be termed as voltage stability (Kundur 1994). The dynamics of voltage collapse could range from a few seconds to tens of minutes. So, depending upon the duration of dynamics, there are mainly two-time frames for voltage stability namely transient and the long term (CIGRE Task Force 38.02.10 1993).

- Transient voltage collapse includes the dynamics of fast acting loads such as induction motor or HVDC converters and the time period is one to several seconds.
- Long term voltage collapse involves slow acting load components such as LTC[1] transformers, thermostat-controlled loads and generator excitation limiters. The time frame ranges from 0.5 to 30 minutes (CIGRE Task Force 38.02.10 1993).

[1]The Load tap changing (LTC) is also sometimes referred by other names such as On-load tap changing (OLTC) and Under-load tap changing (ULTC).

.

3 Case study

3.1 Description of a test system

The Kundur-10 bus test system (Kundur 1994) is chosen in order to analyze the performance and influence of different power system components in voltage stability. The test system used for the study is actually based on the system described in (CIGRE Task Force 38.02.08 1995) as BPA[2] test system, with some changes in load and compensating devices parameters. The single line diagram of the test system is shown in Figure 1. The necessary data used for the simulation of the system is provided in Section A.

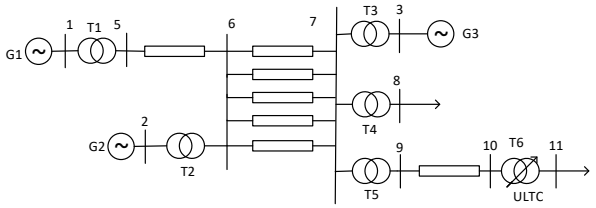

Figure 1. Single line diagram of test system (CIGRE Task Force 38.02.08 1995).

Here the generators G1 and G2 in remote areas supply loads to the local area through five 500 kV transmission lines. The local generator G3 at bus 3 generates 1154 MW and the remaining power is supplied by two remote generators. Shunt capacitors are placed at various locations in the local area. Figure 2 shows the implementation of test system in PSAT.

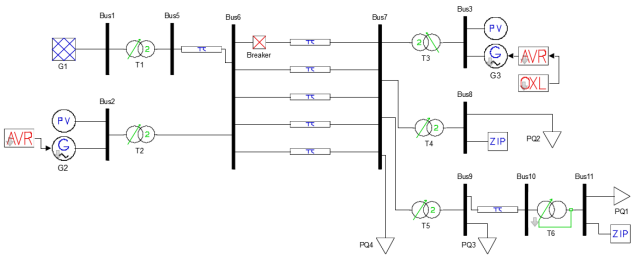

Figure 2. Single line diagram implementation of test system in PSAT.

The steady state voltage profiles and reactive power at different buses are shown in figure 3 and 4 respectively.

3.2 System Modelling

For the test system, the loss of one of the transmission lines between bus 6 and bus 7 is considered as a disturbance during the simulation.

Generators G2 and G3 are modelled using 6th order model of PSAT whereas the generator G1 is modelled as an infinite bus.

[2]Bonneville Power Administration `https://www.bpa.gov`

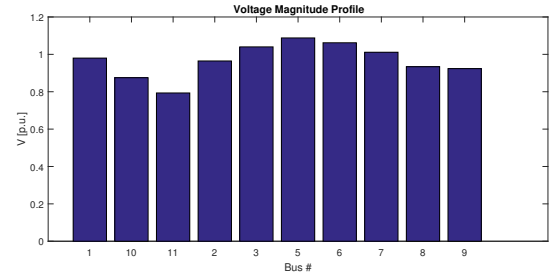

Figure 3. Steady state voltage at various buses.

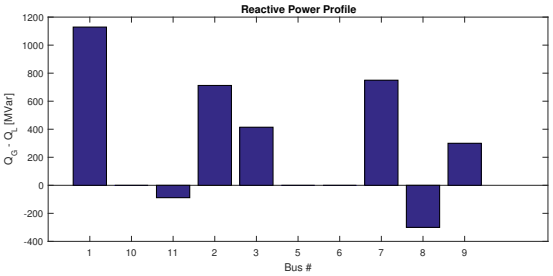

Figure 4. Steady state reactive power at various buses.

Load at bus 8 is modelled as constant power for both active and reactive power whereas the load at bus 11 is modelled as constant impedance load for both active and reactive power as represented by PQ2 and PQ1 load respectively in Figure 2. The shunt capacitors at buses 7, 8 & 9 are modeled as PQ load (PQ4, PQ2, PQ3) respectively with the values presented in Table 2.

Transformer LTC performance is characterized by deadband and step size. The deadband is taken as $\pm 1\%$ p.u. of bus voltage to which LTC is controlling and the tap range is ± 16 steps with a step size of 5/8%. The integral deviation H and inverse time constant K for the system is taken as 0.001 p.u. and 0.10 per second respectively. Figure 5 and Figure 6 shows the equivalent π circuit model and secondary voltage control scheme of LTC transformer respectively.

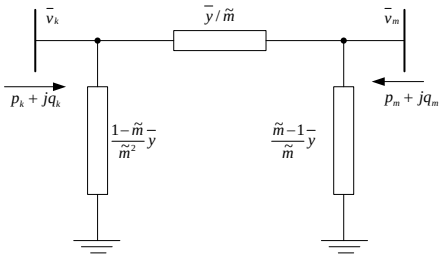

Figure 5. Equivalent π circuit of Under Load Tap Changer (Milano 2013)

Over Excitation Limiter is included for generator G3 only, for this case study. Figure 7 shows a PSAT model of overexcitation limiter used in the test system. The integrator time constant T_o for the limiter is taken as 60 seconds

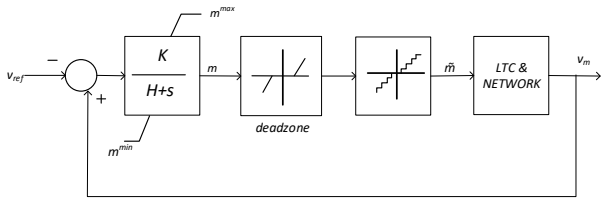

Figure 6. Secondary voltage control scheme of LTC (Milano 2013).

whereas the maximum field current limit is chosen as 11.7 p.u. for the test system.

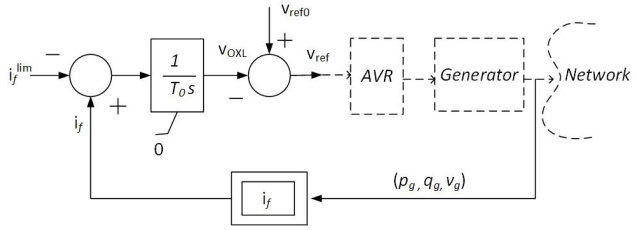

Figure 7. Over excitation limiter (Milano 2013).

3.3 Simulation Results

The voltage at various buses and the reactive power outputs of the generator is compared for the test system including and excluding the over excitation limiter with ULTC in action for both cases which are as presented in the Figures from 8 to 12.

The sequence of events triggered during the simulation in different time frames can be explained as follows.

- One of the transmission lines is disconnected at time t=5 seconds. When the line has been disconnected, the apparent impedance and consequently the line losses and voltage drop of the transmission system is increased.

- The second time frame starts at around 10 seconds where the ULTC is activated as the voltage at the bus 11 is lower than the preset value. The ULTC tries to keep the voltage at the secondary bus (bus-11) at its original value by adjusting its tap ratio which demands more reactive power support from the generators present in the network. Thus, to meet the increased reactive power demand the excitation current is continuously increased until the maximum tap of transformer is reached or voltages at the buses are recovered. This time frame can be observed in sub-figures from 8a-12a. The voltage at bus 11 is restored to nearly its reference value in about 90 seconds as shown in Figure 8.

- The third time frame begins with the actuation of overexcitation limiter as shown in sub-figure 8b at around t=150 seconds by ramping down the field current. The following chains of events occurs after the actuation of OXL:

  – As the field current of G3 is reduced, its terminal voltage drops.
  – Voltages at bus 11, 10 and 7 drops.
  – ULTC on T6 tries to restore the voltage at bus 11 back to its original value.
  – The reactive power demand on generators increases. Field current of machine 3 increases and continues to remain at its limit and the terminal voltage of G3 further decreases.
  – Voltage at bus 7 drops and causes a further reduction in terminal voltage of bus 10 and bus 11.
  – The ULTC operates again, repeating above mentioned chains of events.

  Hence in response to each tap movement of ULTC, the voltage at bus 11 reduces rather than increased. This indicates that the system has entered into the voltage instability phase. The bus 11 voltage falls progressively as shown in Figure 8b until the ULTC reaches its maximum tap position at around 260 seconds. The voltage at bus 11 settles at around 0.77162 p.u.

Furthermore, the effect of static load models on long term voltage stability was studied for the test case considered. Figure 13 shows the voltage profile at bus 11 when the load at bus 8 is modelled as constant impedeance, constant current and constant power load keeping the load at bus 11 as constant impedeance. The ULTC and OXL were kept inactive during this condition and transformer T6 is implemented as a fixed tap transformer with tap ratio same as that of transformer T5.

It is observed that the constant power load stabilizes at a lower value as compared to constant impedance and constant power load because of its load restoring characteristics (Nguyen 2008). That means constant power load tries to consume the same power at a pre-disturbance level as consumed power is independent of voltage variations and hence the voltage drops even further. The dynamics of voltage profile obtained is comparable to the similar case study performed in Ph.D. thesis (Nguyen 2008) using PSS/E software.

4 Generator PQ capability curve

Synchronous generator is a primary source of reactive power in the network and plays an important role in maintaining the voltage stability in the network. The boundaries for supplying the reactive power at a given active power output is defined by the generator capability curve provided by the manufacturers (Dragosavac et al. 2012). The generator capability diagram provides a boundary

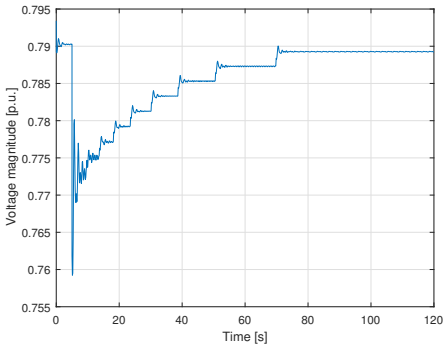

(a) With only ULTC

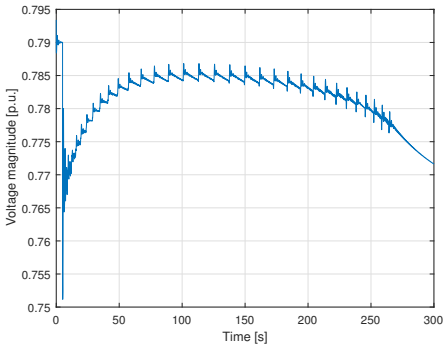

(b) With ULTC and OXL

Figure 8. Bus 11 voltage without and with OXL.

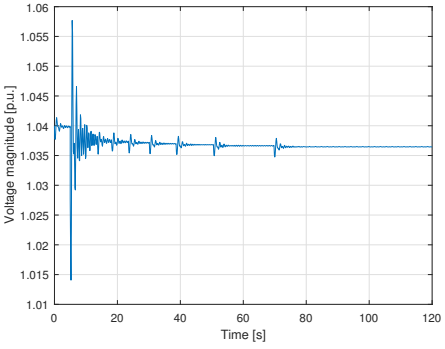

(a) With only ULTC

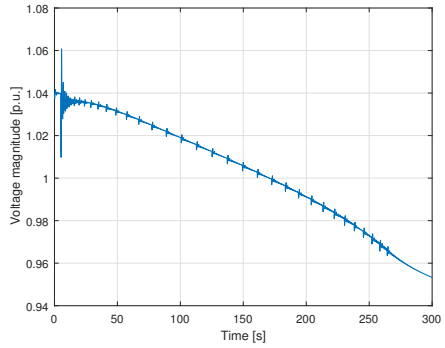

(b) With ULTC and OXL

Figure 10. Bus 3 voltage without and with OXL.

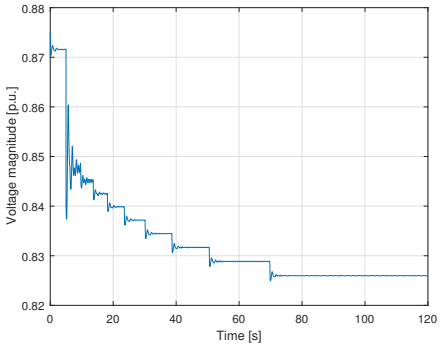

(a) With only ULTC

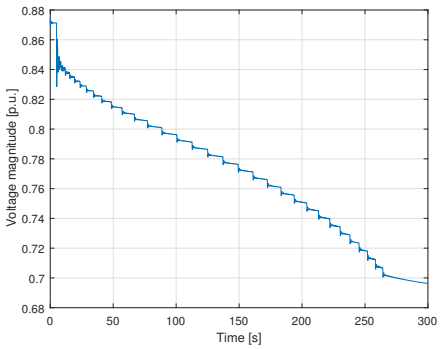

(b) With ULTC and OXL

Figure 9. Bus 10 voltage without and with OXL.

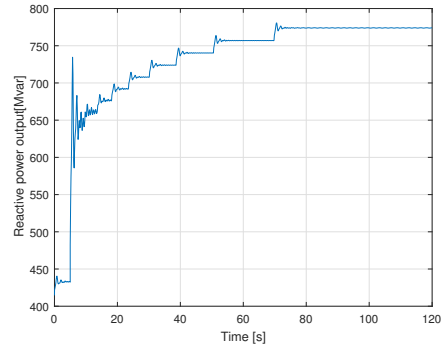

(a) With only ULTC

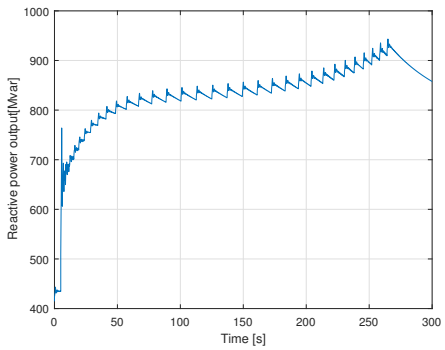

(b) With ULTC and OXL

Figure 11. Reactive power output of generator G3 without and with OXL.

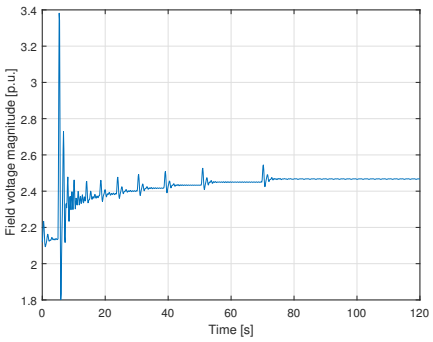

(a) With only ULTC

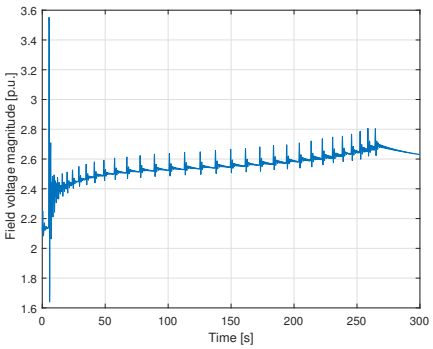

(b) With ULTC and OXL

Figure 12. Field voltage at generator 3 without and with OXL.

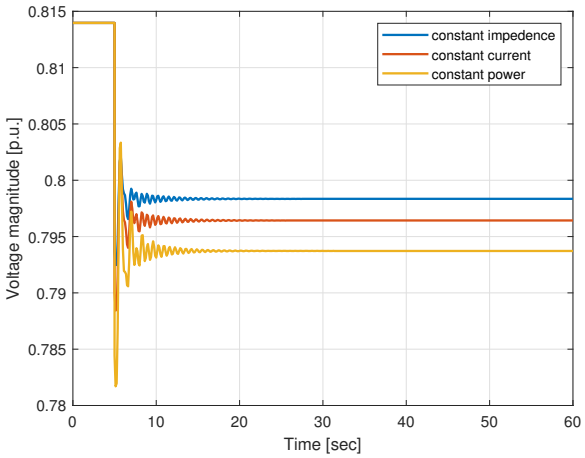

Figure 13. Voltage profile at bus 11 for different load types.

within which the generator can operate safely without exceeding the thermal limitations. Following operational constraints are the reasons for the limits in active and reactive power of the synchronous generator (Machowski, Bialek, and Bumby 2008).

1. Armature current limit.
2. Field current limit.
3. Steady-state stability limit.
4. Stator end region heating limit.
5. Generator active power limit.

This paper presents the methodology for obtaining the PQ diagram for a cylindrical rotor synchronous generator with the following simplification during its modelling:

- The synchronous generator has been assumed to be connected to the infinite bus i.e. with constant voltage.
- The machine saturation effect on the direct axis synchronous reactance has not been considered, i.e. $X_d = \text{constant}$.
- The effect of armature resistance has also been neglected.

The rated parameters of generator G3 in local area in the 10-bus system is taken as reference for determining capability diagram with 10% stability margin.

The theoretical PQ diagram can be derived by dividing every phasor in the vector diagram by direct-axis synchronous reactance X_d and multiplying them with the armature voltage as shown in figure 14. The figure so obtained, contains P and Q as the x-axis and y-axis respectively.

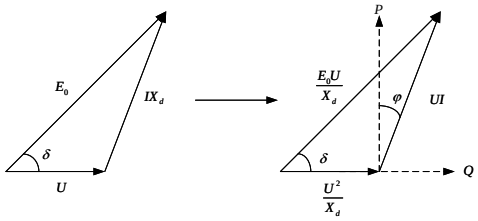

Figure 14. Derivation of a P-Q capability diagram from the phasor diagram (cylindrical rotor) (Vrazic, Viskovic, and Hanic 2014).

4.1 Rated turbine power limit

The maximum and the minimum turbine power limits are drawn according to the following two conditions (I.Ilić et al. 2007):

- If the power of the turbine (P_T) exceeds the rated power of the generator (P_n), i.e. if $P_T > P_n$, then $P_{max} = P_n$.
- If the power of the turbine is equal to or less than the rated power of the generator ($P_T \leq P_n$), then $P_{max} = P_T.\eta_G$.

This limit is shown in Figure 15 labelled as P_{max}. The minimum power depends upon the turbine requirements. For example, in Kaplan and Francis turbine minimum power output is 5 % to 30% of rated output whereas in some turbines like Pelton turbine this limitation does not exists (I.Ilić et al. 2007).

4.2 Rated stator current limit

The rated stator current limit is plotted as a constant semi-circle with center at origin '0' and radius as the rated apparent power, S_n as shown in Figure 15. Point 'P' denotes the rated operating condition of the generator which is defined at its rated power factor $cos\phi_n = 0.72$. So,
$P_{rated} = S_n cos\phi = 1 * 0.72 = 0.72$ p.u.
$Q_{rated} = S_n sin\phi = 1 * \sqrt{1-(cos\phi)^2} = 0.69$ p.u.

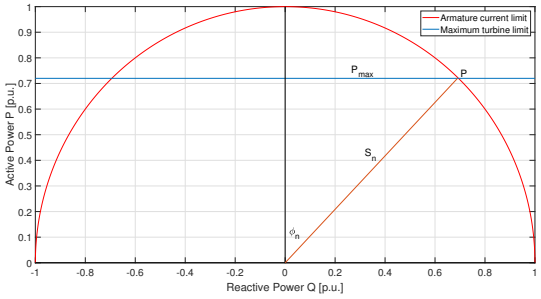

Figure 15. Rated stator current limit and maximum turbine limit plot.

4.3 Rated field current limit

For implementing the rated field current limit, an arc is drawn with the center at (0,-$\frac{V^2}{x_d}$) and radius $\frac{E_{qmax}V}{x_d}$ from $cos\phi = 0$ to $cos\phi = 0.72$ (rated) where E_{qmax} is calculated from the phasor diagram as shown in Figure 14 as:

$$E_{qmax} = \sqrt{(V + Ix_d sin\phi)^2 + (Ix_d cos\phi)^2}\ \text{pu} \qquad (1)$$

The limit is drawn as curve PK in Figure 16.

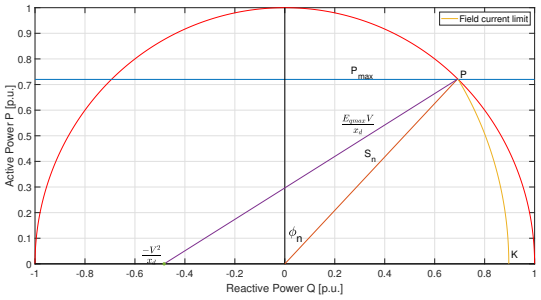

Figure 16. Rated field current limit plot.

4.4 Practical Stability limit

For round-rotor generators, theoretical stability limit is achieved at load angle δ=90°. However, the theoretical stability curve is reduced by a constant power value, for example by 10% of the rating of the machine as a safety margin and the corresponding curve so obtained is termed as practical stability margin (Walker 1953).

The theoretical stability curve is drawn as a straight line at point (0,-$\frac{V^2}{x_d}$)= (0,-$\frac{1}{2.07}$)= (0,-0.48) represented by

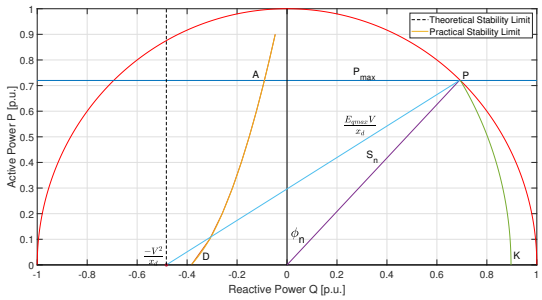

Figure 17. Theoretical and practical stability limit plot.

dashed line in Figure 17. The practical stability limit is represented as curve AD in the same figure.

Hence, the safe region for the operation of a synchronous generator is represented by the area bounded by curve APKD in Figure 17.

5 Visualization tool

As discussed in Section 4, various operational limits in PQ diagram was implemented in MATLAB software environment. For improved visualization of the diagram, a visual App was created using MATLAB App designer. A Graphical User Interface was created by using different components from the component library and specifying app's design and layout. For defining the App behavior, App designer allows an integrated version of the MATLAB Editor (*MATLAB App Designer* 2019). All the parameter values implemented, and the dynamics observed in the visualization tool is based upon the case study of Kundur 10-bus test system described in Section 3.1.

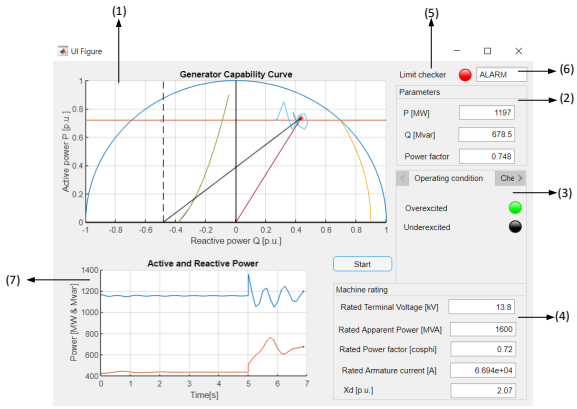

Figure 18. Graphical User Interface for generator capability diagram.

Figure 18 shows a GUI environment for the designed App in order to visualize the generator capability. The GUI consists of two figure windows and three tabs. The upper figure (1) in the user interface shows the capability curve with the real-time operating point as indicated by 'red' asterisk symbol. The 'Parameters' tab (2) shows the operating point (P and Q) values in real time along with

the operational power factor. The 'Operating conditions' tab (3) shows the actual operating condition i.e. whether the generator is operating in over excitation mode or under excitation mode with current operation mode indicated by lamp glowing 'green'. The 'Machine rating' tab (4) indicates the generator rated conditions which can be changed by changing the values in the respective fields. For example, the effect of change of direct axis synchronous reactance on the generator limits can be visualized in the figure section (1) by changing its value in the 'Machine rating' tab.

On top of the 'Parameters' tab resides a 'Limit checker' (5) as indicated by a lamp which glows 'red' when the defined operational limits on the capability curve are violated along with the actuation and information of 'ALARM' (6) to notify the operating personnel about the limit violation as shown in Figure 18. The lamp glows 'green' along with an information 'NORMAL' when the operating point lies within the defined boundaries as shown in Figure 19.

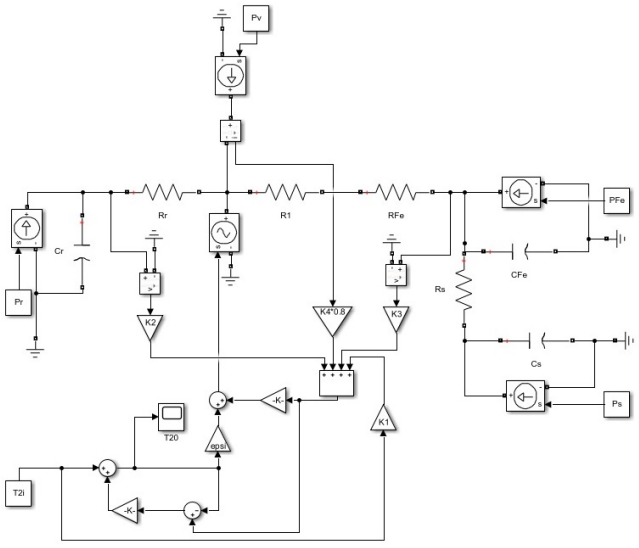

Figure 20. Simulink circuit for the thermal model proposed in (Øyvang, Noland, et al. 2018).

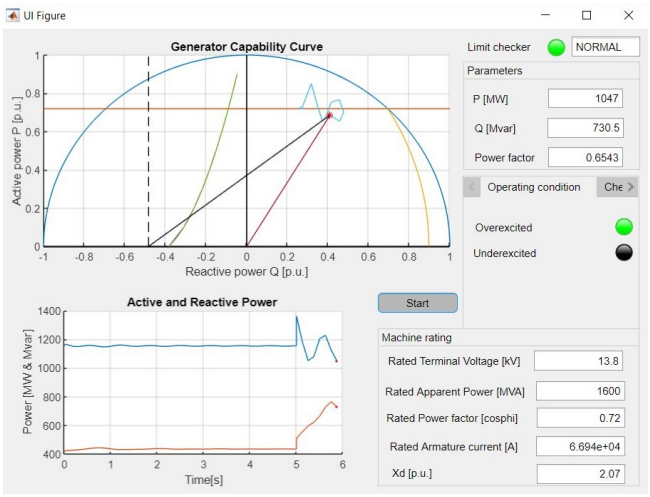

Figure 19. Graphical User Interface for Generator Capability Diagram showing 'NORMAL' condition.

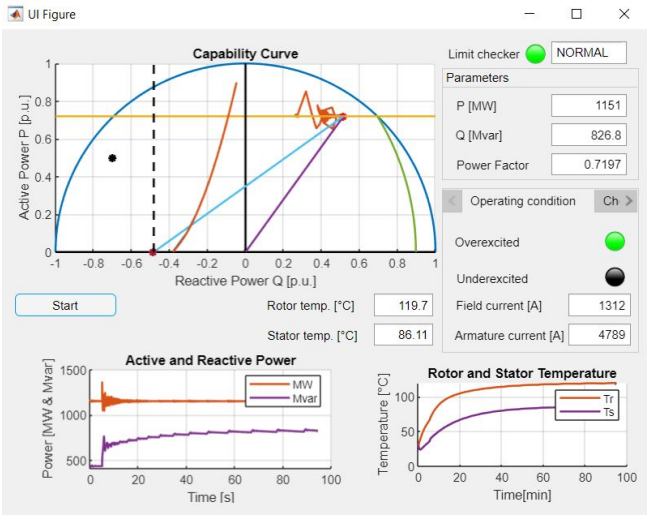

Figure 21. Temperature observation in the visualization tool.

5.1 Temperature visualization

The temperature development in the stator and rotor windings in the synchronous generator was also observed in the same tool which is as shown in Figure 21 using the thermal model as described in Ph.D. thesis (Øyvang, Noland, et al. 2018). Figure 20 shows the thermal model implemented in Simulink software environment. The output temperatures as seen in the figure is the result of input field current and armature current taken from the local generator G3 in Kundur 10-bus system when replaced by 103 MVA hydrogenerator at 'Åbjøra' in Norway. The machine data of hydrogenerator is provided in Table 6. The field and the stator currents in real time are observable in the tool. The initial temperature in the stator and rotor was taken as 28°C during the simulation.

6 Conclusion and further work

The dynamic analysis of voltage stability using time-domain simulation has been presented in this paper using a test power system containing 10 buses as a case study. From the simulation, it can be concluded that dynamic analysis is very useful in understanding the detail dynamics involved during the larger disturbances such as a loss of transmission line or loss of generation in the system and to study the coordination between the control and the protection as well. This type of analysis gives accurate results though it requires detail accurate models of the components and is time-consuming. The influence of static load models on the voltage collapse scenario is well-presented in this paper. The severity of the effect depends upon the type of load.

The development and implementation of PQ capabil-

ity diagram for the cylindrical rotor machine was done in MATLAB. The use of Graphical User Interface provides the user interaction with the visualization tool through graphical displays, inputs and visual indicators. During implementation, the infinite bus-bar assumption was made which is not practical in real case as the terminal voltage can significantly vary from the rated value. As the terminal voltage varies, the field and the armature limits also vary. Furthermore, the assumption of constant direct-axis synchronous reactance is also not valid as the synchronous machine are designed with certain amount of saturation level and depends upon machine operating point such as armature voltage and current (Vrazic, Viskovic, and Hanic 2014).

The effect of dynamic load characteristics which has a significant influence on voltage stability can be analyzed under further work. Moreover, other simulation tools like PSS/E, DIgSILENT PowerFactory, EUROSTAG, SimPowerSystems, EPRI Extended Transient Mid-Term Stability Program (ETMSP) can be used to test and compare results from the same test system for voltage instability and collapse phenomena.

A Data for Test System

S_{base} = 100 MVA

Table 1. Bus Data

Bus	*Base [kV]*	*Vscheduled [p.u.]*	*Phase [rad]*	*Shunt [Mvar]*	*P load [MW]*	*Q load [Mvar]*
Bus1	13.8	0.98	0	0	0	0
Bus2	13.8	0.96	0	0	0	0
Bus3	13.8	1.04	0	0	0	0
Bus5	500	1.00	0	0	0	0
Bus6	500	1.00	0	0	0	0
Bus7	500	1.00	0	750	0	0
Bus8	13.8	0.94	0	1500	3000	1800
Bus9	115	0.95	0	300	0	0
Bus10	115	0.89	0	0	30	0
Bus11	13.8	0.91	0	0	3100	90

Table 2. Generators load flow data

Bus No.	*Gen Name*	*Base [kV]*	*P gen [MW]*	*Q gen [Mvar]*	*Sbase [MVA]*	*Qmax [Mvar]*	*Qmin [Mvar]*
1	G1	13.8	3471.9	1129.03	5000	1600	-1000
2	G2	13.8	1736	712.53	2200	725	200
3	G3	13.8	1154	414.58	1600	700	-100

Machine parameters:
Machine 1: Infinite bus
Machine 2: H = 2.09, MVA rating = 2200 MVA
Machine 3: H = 2.33, MVA rating = 1400 MVA

Following are the parameters for machine 2 and machine 3 on their respective MVA ratings:

$$R_a = 0.0046 \quad X_d = 2.07 \quad X_q = 1.99$$
$$X_l = 0.155 \quad X'_d = 0.28 \quad X'_q = 0.49$$
$$X''_d = 0.215 \quad X''_q = 0.215$$
$$T'_{do} = 4.10 \quad T'_{qo} = 0.56$$
$$T''_{do} = 0.033 \quad T''_{qo} = 0.062$$

Table 3. Transmission lines data

From Bus	*To bus*	*R [p.u.]*	*X [p.u.]*	*B [p.u.]*
5	6	0.0000	0.0040	0.0000
6	7	0.0015	0.0288	1.1730
9	10	0.0010	0.0030	0.0000

Table 4. Transformers data

Transformer	*R [p.u.]*	*X [p.u.]*	*Tap ratio*
T1	0.0000	0.0020	0.8857
T2	0.0000	0.0045	0.8857
T3	0.0000	0.0125	0.9024
T4	0.0000	0.0030	1.0664
T5	0.0000	0.0026	1.0800
T6	0.0000	0.0010	0.9750

Table 5. Thermal model data

Parameters	*Symbol*	*Value*	*Unit*
Thermal resistance, $T_{Fe} - T_{\delta}$	R_{Fe}	0.07	K/kW
Thermal resistance, $T_s - T_{Fe}$	R_s	0.05	K/kW
Thermal resistance, air	R_1	0.018	K/kW
Gain coefficient, $T_{2,i}$	K1	0.59	-
Gain coefficient rotor(Cu)	K2	0.5	-
Gain coefficient stator(Fe)	K3	0.36	-
Heat exchanger effieicency (epsi)	ε	0.595	-

Table 6. Machine data of Åbjøra (Øyvang, Hegglid, and Lie 2018).

Description	*Parameters*	*Value*	*Unit*
Rated power	S_n	103	MVA
Rated voltage	V_{tn}	11	kV
Rated current	I_{tn}	5406	A
Rated field current	I_{fdn}	1064	A
Inertia constant	H	2.66	s
Number of polepairs	p	6	-
Synchronous reactance d-axis	x_d	1.09	[p.u.]
Synchronous reactance q-axis	x_q	0.67	[p.u.]
Transient reactance d-axis	x'_d	0.24	[p.u.]
Subtransient reactance d-axis	x''_d	0.15	[p.u.]
Subtransient reactance q-axis	x''_q	0.19	[p.u.]
Transient OC Time constant d-axis	T'_{do}	10	s
Transient OC Time constant q-axis	T'_{qo}	0.23	s
Subtransient OC Time constant d-axis	T''_{do}	0.086	s
Subransient OC Time constant q-axis	T''_{qo}	0.23	s
Stator leakage inductance	X_l	0.08	[p.u.]
Stator resistance	R_a	0.00182	[p.u.]

Exciters: Both machine 2 and machine 3 uses thyristor exciters with a gain of 100 and the time delay of the measurement system as 0.02 seconds.

Overexcitation limiter for machine 3: The OXL model used in the simulation is as described in the section...with integrator time constant (T_0)= 60 seconds, maximum field current i_{fd}^{lim}= 11.7 p.u. and maximum output signal $v_{OXL}^{\max}$= 5.02 p.u.

ULTC data for transformer T6 between bus 10 and 11:

Deadband: ± 1 % p.u. bus voltage
Tap range: ± 16 steps
Step size: 5/8 % (=0.00625 p.u.)

References

CIGRE Task Force 38.02.08 (1995). *Long Term Dynamics Phase II*. Tech. rep. CIGRE.

CIGRE Task Force 38.02.10 (1993). *Modelling of Voltage Collapse Including Dynamic Phenomena*. Tech. rep.

Dragosavac, J. et al. (2012). "On-line Estimation of Available Generator Reactive Power for Network Voltage Support". In: *8th Mediterranean Conference on Power Generation, Transmission, Distribution and Energy Conversion (MEDPOWER 2012)*. Institution of Engineering and Technology. DOI: 10.1049/cp.2012.2014.

I.Ilić et al. (2007). "Methodology for Determining the Actual PQ Diagram of a Hydrogenerator". In: *Journal of Energy* 56.2, pp. 144–181. URL: https://hrcak.srce.hr/13153.

Kundur, Prabha (1994). *Power System Stability and Control*. McGraw-Hill, Inc.

Machowski, Jan, Janusz W. Bialek, and James R. Bumby (2008). *Power System Dynamics : Stability and Control*. 2nd ed. John Wiley & Sons, Ltd.

MATLAB App Designer (2019). URL: https://se.mathworks.com/products/matlab/app-designer.html (visited on 03/22/2019).

Milano, Federico (2013). *Power System Analysis Toolbox Documentation for PSAT*. Version 2.1.8.

Nguyen, Dang Toan (2008). "Contributions to analysis and prevention of power system blackouts". Theses. Institut National Polytechnique de Grenoble - INPG. URL: https://tel.archives-ouvertes.fr/tel-00352414.

Øyvang, Thomas (2018). "Enhanced power capability of generator units for increased operational security". PhD thesis.

Øyvang, Thomas, Gunne J. Hegglid, and Bernt Lie (2018). "Models of synchronous generators with excitation system, for transient power system studies". In: *IFAC-PapersOnLine* 51.2, pp. 91–96. DOI: 10.1016/j.ifacol.2018.03.016.

Øyvang, Thomas, Jonas Kristiansen Noland, et al. (2018). "Online Model-Based Thermal Prediction for Flexible Control of an Air-Cooled Hydrogenerator". In: *IEEE Transactions on Industrial Electronics*, pp. 1–1. DOI: 10.1109/tie.2018.2875637.

Vrazic, M., A. Viskovic, and Z. Hanic (2014). "User P-Q Diagram as a Part of a Synchronous Generator Monitoring System". In: *Electronics and Electrical Engineering* 20.4. DOI: 10.5755/j01.eee.20.4.5333.

Walker, J.H. (1953). "Operating characteristics of salient-pole machines". In: *Proceedings of the IEE - Part II: Power Engineering* 100.73, pp. 13–24. DOI: 10.1049/pi-2.1953.0004.